Power Management Circuit Design for Vibration Energy Harvesting from Freight Railcars

Thomas Joseph O'Connor III

Thesis submitted to the faculty of the
Virginia Polytechnic Institute and State University
in partial fulfillment of the requirements for the degree of

Master of Science
In
Electrical Engineering

Dong S. Ha, Chair
Qiang Li, Co-Chair
Mehdi Ahmadian

May 4, 2015
Blacksburg, VA

Keywords: Inverting Buck-Boost Converter, Vibration Energy Harvesting, Battery Management, One-Cycle Control, Maximum Power Transfer, Constant Input Impedance

Power Management Circuit Design for Vibration Energy Harvesting from Freight Railcars

Thomas Joseph O'Connor III

ABSTRACT

Although the locomotive of a train is energized, in general, other railcars are not. This prevents commercial rail companies from installing sensor equipment on the railcars. Thus, several different solutions have been proposed to provide energy for commercial railcars. One such solution is a vibration-based energy harvester which can be mounted in the suspension coils of the railcar. The harvester translates the linear motion of the suspension vibration into rotational motion to turn a 3-phase AC generator. When subjected to real-world suspension displacements, the harvester is capable of generating peak energy levels in excess of 70 W, although the average energy harvested is much lower, around 1 W.

A battery pack can be used to store the useful energy harvested. However, a power conditioning circuit is required to convert the 3-phase AC energy from the harvester into DC for the battery pack. The power converter should be capable of extracting maximum power from the energy harvester as well as acting as a battery manager. Experimental results with the energy harvester conclude that maximum power can be extracted if the harvester is loaded with 2 Ω. In order to maintain a constant input impedance, the duty cycle of the power converter must be fixed. Conversely, output regulation requires the duty cycle to change dynamically. Consequently, there is a tradeoff between extracting maximum power and prolonging the battery life cycle. The proposed converter design aims to achieve both maximum power transfer and battery protection by automatically switching between control modes.

The proposed converter design uses an inverting buck-boost converter operating in discontinuous conduction mode to maintain a constant input impedance through a fixed duty cycle. This constant input impedance mode is used to extract maximum power from the harvester when the battery is not close to fully charged. When the battery is near fully charged, extracting maximum power is not as important and the duty cycle can be controlled to regulate

the output. Specifically, one-cycle control is used to regulate the output by monitoring the input voltage and adjusting the duty cycle accordingly. Finally, the converter is designed to shut down once the battery has been fully charged to prevent overcharging. The result is a power converter that extracts maximum power from the energy harvester for as long as possible before battery protection techniques are implemented. Previous related studies are discussed, tradeoffs in converter design are explained in detail, and an experimental prototype is used to confirm operation of the proposed control scheme.

To my parents, sisters, and grandparents

Acknowledgements

I would like to thank my advisor, Dr. Dong S. Ha, for being my mentor, teacher, and friend throughout the undergraduate and graduate process. Dr. Qiang Li's knowledge and expertise has also been invaluable during my graduate studies and I could not be more grateful for his assistance. I would also like to thank Dr. Mehdi Ahmadian for being part of my advisory committee and improving my skills to become an overall better engineer.

I offer my sincerest gratitude to Virginia Tech, I could not ask for a better academic environment to spend the last six years immersed in. Additionally, I would like to thank the Center for Vehicle Systems and Safety and the Railway Technologies Laboratory at Virginia Tech, without whom I would not have made it this far. I would also like to thank Eric Yates and Linear Technology for quickly providing me with sample components which were used in the final prototype design.

A special thanks is reserved for my close colleagues Brian Cassidy, Taylor Yeago, Ross Kerley, and Dan Ridenour for working with me to better understand electrical concepts and being there to talk through difficult problems with. I'd also like to thank my colleagues in the MICS lab, whom I'm sure will be further improving the MICS name with great research accomplishments in the years to come.

I'd also like to thank Markus Kusano, Eliza Schlein, and Kevin McDermott, for being great friends who kept me grounded despite the inevitable stress endured throughout graduate school.

Finally, I'd like to thank my parents, Jeanne and Tom, for supporting me my entire life and giving me great advice when I needed it most. My sisters, Kaitlin and Jen, as well as my brother-in-law Barry have also been invaluably supportive and I cannot thank them enough. My sincere thanks also go out to anyone whom I have shamefully forgotten.

Table of Contents

List of Figures

List of Tables

Chapter 1

Introduction

1.1 Motivation

The U.S. freight rail industry is one of the most dynamic freight systems in the world, moving more freight than any other freight rail system on Earth. U.S. freight rail industry, estimated to be worth $60 billion, consists of over 140,000 miles of rail and is responsible for employing over 220,000 people [1]. Innovation is a driving force behind the freight rail industry, and although freight train technology has existed for more than a century, the industry would not be where it is today without constantly adopting new technologies.

One desire of the freight rail industry is to provide power to individual freight rail cars. Typically, the locomotive has plenty of power, but the rail cars are not electrified, which often prevents the rail cars from being equipped with maintenance equipment, sensor networks, or tracking equipment such as GPS or active RFID tags. A self-sustaining system capable of generating electricity for these additional features without affecting normal rail operation is highly desirable to the freight rail industry. One such possible solution is a vibration-based energy harvester developed by the Railway Technologies Laboratory (RTL) at Virginia Polytechnic Institute and State University (VT). The developed energy harvester is capable of generating peak power levels of up to 140 W [2] [3]. The goal of this energy harvester is to be placed within or alongside the suspension coils of a freight railcar to harvest energy from the displacement of the suspension while the rail car is in motion. With the addition of a power converter at the output of the energy harvester, the power generated can be conditioned and stored into a high-capacity battery pack. This research project addresses the development of a unique power converter capable of fulfilling the distinct needs of this application.

1.2 Scope of the Proposed Research

The harvester produces energy by translating the linear motion of the suspension displacement into rotational motion which turns a 3-phase AC generator. Previous experimental testing of the harvester's capabilities has been performed with using a diode bridge rectifier and resistive load to measure the power output levels corresponding to different linear displacement magnitudes of the harvester. A DC-to-DC converter can be added after the diode bridge rectifier to condition the pseudo-DC waveform for storage into the battery pack.

Electromagnetic generators, such as the one used in the design of this energy harvester, generate the most power when they are connected to a resistively matched load. The duty cycle of a DC-to-DC converter can be fixed to maintain a constant input impedance and emulate a resistive load. However, fixing the duty cycle of a DC-to-DC converter severely limits the converter's ability to respond to different transient events. For example, the duty cycle of the converter needs to be dynamically adjusted to maintain a constant output voltage if the input voltage magnitude changes. In addition, for a power converter to act like a battery charger, the duty cycle needs to be controlled in order to achieve common battery charging modes. Thus, a converter design for this application has a conflict where the duty cycle must be kept constant in order to achieve maximum power transfer from the energy harvester, but the duty cycle must also change dynamically to properly charge the battery pack and respond to different input voltage magnitudes.

Related previous studies on vibration-based energy harvesting focus primarily on optimizing the energy harvested through more efficient conversion methods and topologies. Additionally, previous studies related to battery charging techniques focus primarily on how to charge the battery without damaging it, despite the charger being used for energy harvesting purposes. Since there is a tradeoff between a converter functioning as a maximum power extractor or a battery charger, there has not been a study which attempts to combine these functions into a single control scheme for a single stage converter. This study aims to implement a simple control scheme which functions as both a maximum power extractor for the energy harvester as well as a battery manager in a single converter topology approach.

1.3 Proposed Approach and Technical Contributions

A power converter targeted for converting the energy generated by the RTL vibration-based energy harvester and storing the harvested energy into a battery pack was designed and prototyped. The major design objectives of the converter is to extract maximum power from the harvester, maintain efficient energy conversion, and protect the battery using standard battery charging techniques. Technical contributions of the proposed research are as follows.

First, the power stage of the converter was designed to meet the objectives for the target application. The inverting buck-boost topology operating in Discontinuous Conduction Mode is adopted to maintain a constant input impedance and extract maximum power from the harvester. Component selection for all aspects of the power stage was discussed in detail, with focus on maintaining an efficient power stage.

Second, a control network was successfully designed and implemented to operate the power converter in different modes to achieve the design objectives. Specifically, one-cycle control (OCC) was adopted to control the conversion rate of power from the sporadically changing energy harvester voltage level to the comparatively static voltage level of the battery. A control selection network was designed to select between different modes of operation: constant input impedance mode for maximum power transfer, output regulation mode for battery protection and improved efficiency, and overvoltage shutdown mode for when the battery is fully charged. The different operating modes are dependent on the voltage charge level of the battery pack, thus the control network is a combination of feedforward and feedback control.

Third, the proposed converter design is prototyped using readily available discrete components. Since the proposed control network is unique to this application and no off-the-shelf controller exists which perfectly fits this application, the control design is also prototyped using discrete components. The prototype demonstrates proper operation of each of the control modes as well as proper selection between the control modes. The prototype reasonably meets the proposed design objectives of maintaining maximum power transfer, providing battery protection, and maintaining efficient power conversion.

1.4 Organization of this Thesis

The organization of this thesis is as follows. Chapter 2 provides background information for the proposed research work, including notable previous studies with related research topics. This chapter discusses important characteristics about the energy harvester which the power converter will be designed for, different DC-to-DC converter topologies and their operation modes, typical approaches to vibration-based energy harvesting, and common battery charging methods. Chapter 3 introduces the proposed inverting buck-boost design as well as the control network. The chapter discusses the design of the power stage, implementation of each of the control modes, selection between the control modes, and guidelines for component selection. The converter is designed to operate in constant impedance mode when the battery is below a certain charge level, switch to output regulation mode when the battery is near fully charged, and shutdown when the battery is fully charged. Chapter 4 presents prototyped converter and measured results from the prototype. Measured results include power consumption of the control network, efficiency of the power stage, and control mode alternation. Finally, Chapter 5 draws conclusions on the proposed controller design as well as suggesting possible future improvements.

Chapter 2

Preliminaries

This chapter presents preliminary information about the energy harvester, DC-to-DC converters, relevant previous research activities, and battery charging techniques. This introductory knowledge is necessary to understand the design approach taken with the proposed converter. Section 2.1 describes the requirements of the converter based on characteristics of the energy harvester and the battery pack. Section 2.2 illustrates different merits of several common DC-to-DC converter topologies. Section 2.3 highlights previous approaches to converter design for vibration-based energy harvesters. Section 2.4 discusses battery charging techniques. Finally, Section 2.5 summarizes chapter 2.

2.1 Design Requirements

2.1.1 Energy Harvester Characteristics

The vibration-based energy harvester developed by the Railway Technologies Laboratory (RTL) at Virginia Tech translates the linear motion of the suspension displacement to rotational motion using a ball screw. A clutch interface ensures rotation is translated in only one direction although the harvester may move linearly up or down. A gear housing is used to increase the turns ratio in order to spin the rotor of the generator faster [4]. Figure 2.1 shows the internal cross-section of the mechanical elements of the energy harvester as well as the completed package of the final prototype energy harvester.

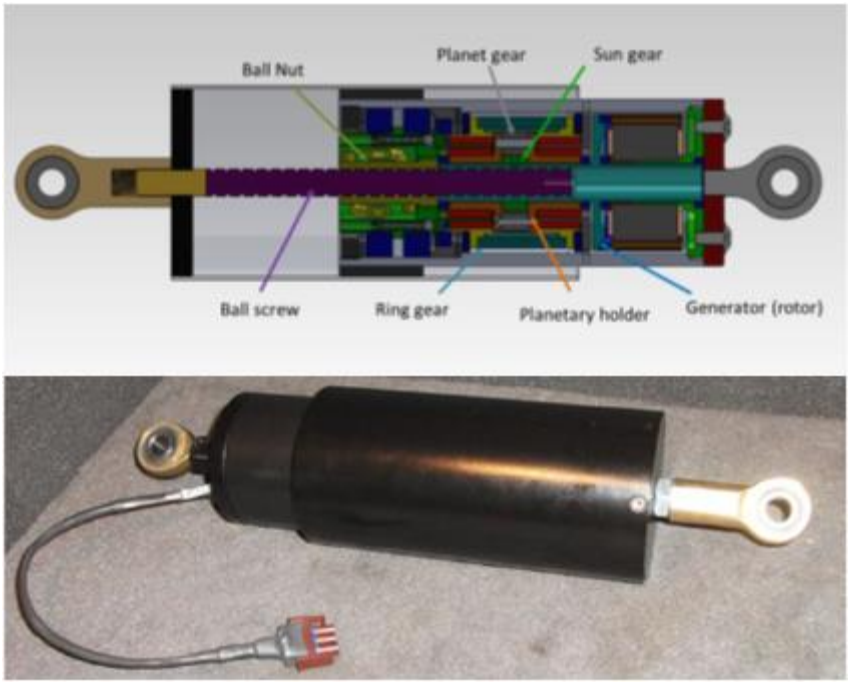

Figure 2.1 Vibration-based energy harvester from C. Nagode, *Electromechanical Suspension-based Energy Harvesting Systems for Railroad Applications,* Ph.D. dissertation, Dept. Mech. Eng., Virginia Tech., Blacksburg, VA, 2013, 2013. Used under fair use, 2015.

The electromagnetic generator of the harvester is made from an off-the-shelf motor, specifically a MonsterPower 160 permanent magnet outrunner brushless DC motor manufactured by Exceed RC. This type of motors, typically used for remote-control airplanes, is used in this application for its compact size and relatively low K_v value, where the K_v value determines the voltage required to spin a motor at a certain speed. Since the motor is used as a generator in this application, a low K_v value is desirable to generate higher voltages at lower rotational speeds.

When used as a generator, the motor generates a three-phase AC output. The generator was characterized using a three-phase diode bridge rectifier and resistive load to measure the output power capabilities of the harvester once its energy was transformed into DC, similar to the method used in [5]. A series of characteristic load tests were performed in order to determine the optimal load resistance which extracts maximum power from the harvester. The output power was measured over a range of load resistance while the energy harvester is subjected to different vertical displacement levels by a hydraulic actuator. illustrates the results of the resistive load testing under different vertical displacement levels. The resistive load will eventually be

replaced with a DC/DC converter and battery load, as shown in Figure 2.3.

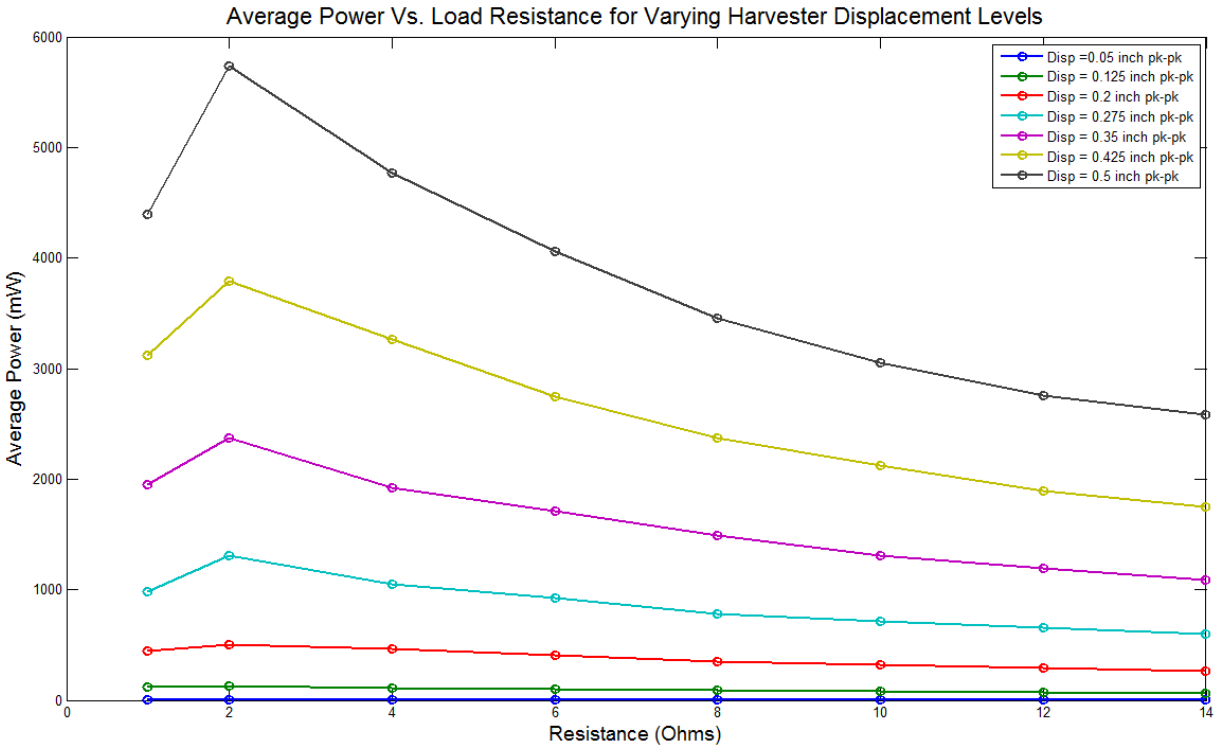

Figure 2.2 Resistive load testing of harvester under different displacement levels.

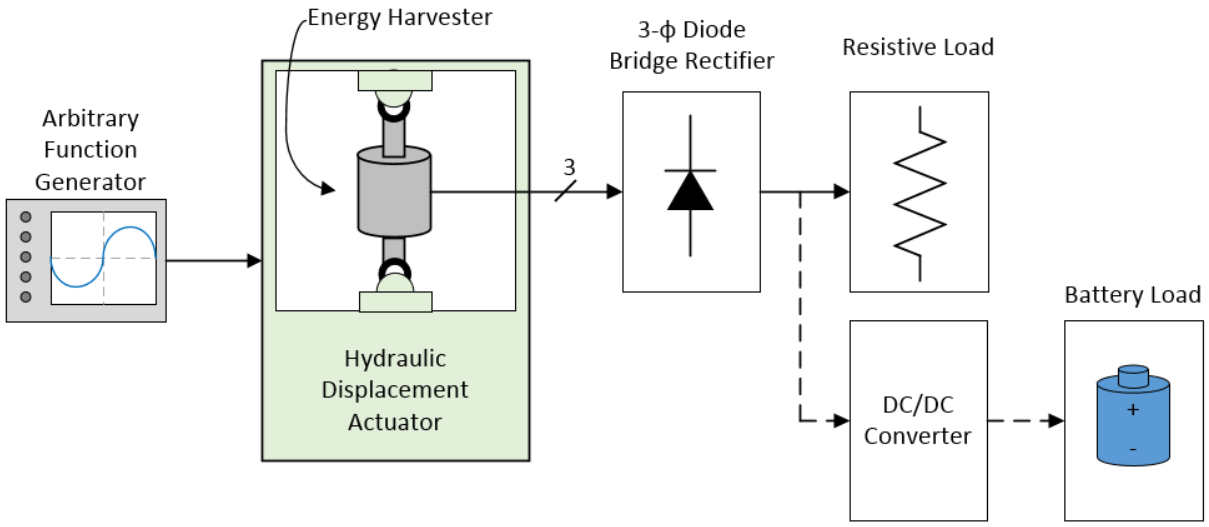

Figure 2.3 Test protocol used to characterize resistive loading of energy harvester.

Two important observations are made about the harvester the resistive load test. First, as expected, the power level for the harvester increases as the vertical displacement is increased. The power level also increases for a higher displacement frequency. Second, the maximum power is extracted from the harvester under the load resistance of 2 Ω. This indicates that

maximum power extraction from the harvester requires the input impedance of the power converter to be a constant of about 2 ohms. This also suggests that maximum power point tracking algorithms are unnecessary, since the peak power output is independent to the displacement level of the harvester.

Nagode tested the harvester on a moving train in order to obtain typical real-world displacement profiles for the harvester [4]. The displacement profile data were loaded to the function generator in Figure 2.3 and the harvester was loaded with a 2 Ω load to determine the output voltage range. Figure 2.4 shows the measured voltage from six different real-world displacement profiles. The profiles show that the peak output is around 12 V and so the peak power output is 72 W, accordingly. There is a possibility for slightly higher or faster displacements onboard the train, so a safety margin is added to the maximum input voltage. Thus, an input voltage range of 0-20 V is considered for the proposed power converter. It is also important to note that the energy harvested under real-world displacement conditions is highly irregular, so if the converter is required to regulate the output, the input voltage must be monitored to adjust the duty cycle according to the input voltage magnitude.

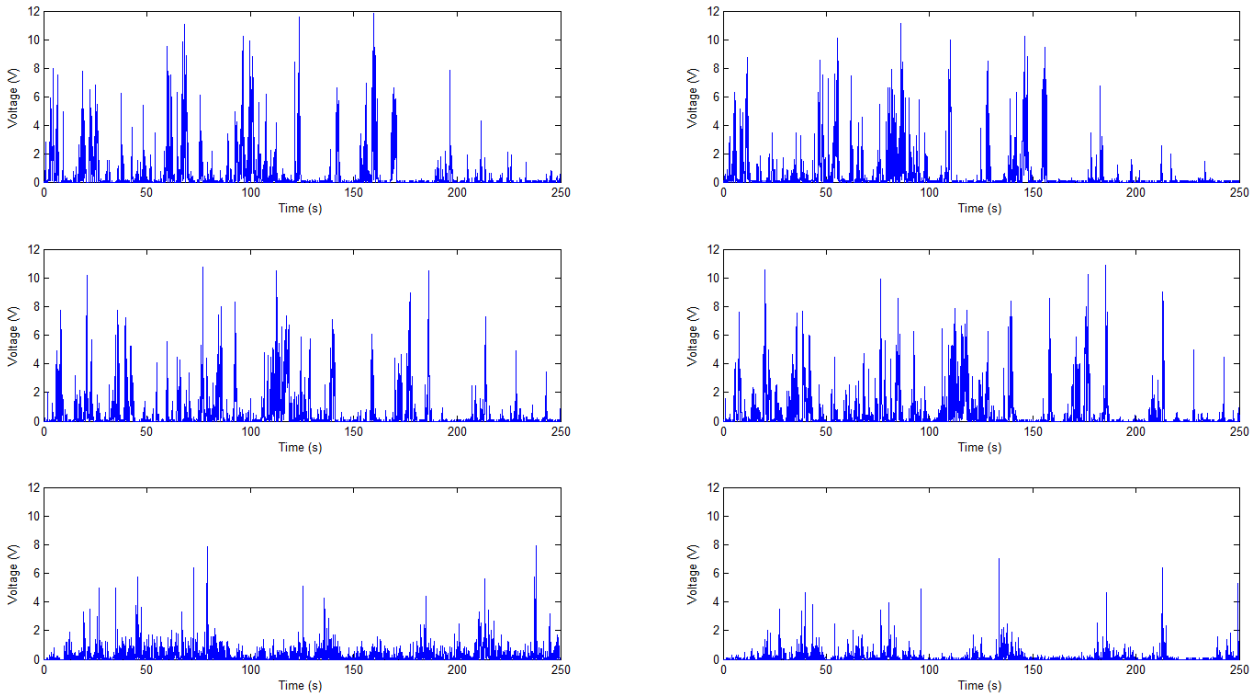

Figure 2.4 Measured energy harvester output voltage under a 2 Ω load.

2.1.2 Battery Load Characteristics

Four LiFePO4 battery cells connected in series, specifically, the 38120S cells manufactured by HeadWay, are used for the proposed design. Each cell has a nominal voltage rating of 3.2 V and a nominal capacity rating of 10 Ah, resulting in a battery pack load of 12.8 V and 10 Ah. These batteries not only boast a large storage capacity, but also are quite rugged and capable of handling maximum charging currents of up to 20 A. The battery discharge curve for a single 38120S cell is shown below in Figure 2.5 [6]. The graph indicates what the voltage level is for the battery while it is being discharged; when the battery is fully charged, the voltage is maximum, but as the battery is depleted the voltage drops. The battery voltage profile indicates that the battery voltage can be used to determine the overall level of charge of the battery. The rise in battery voltage will be monitored to determine what sort of charge level the battery has. Battery charging techniques will be discussed in Section 2.4.

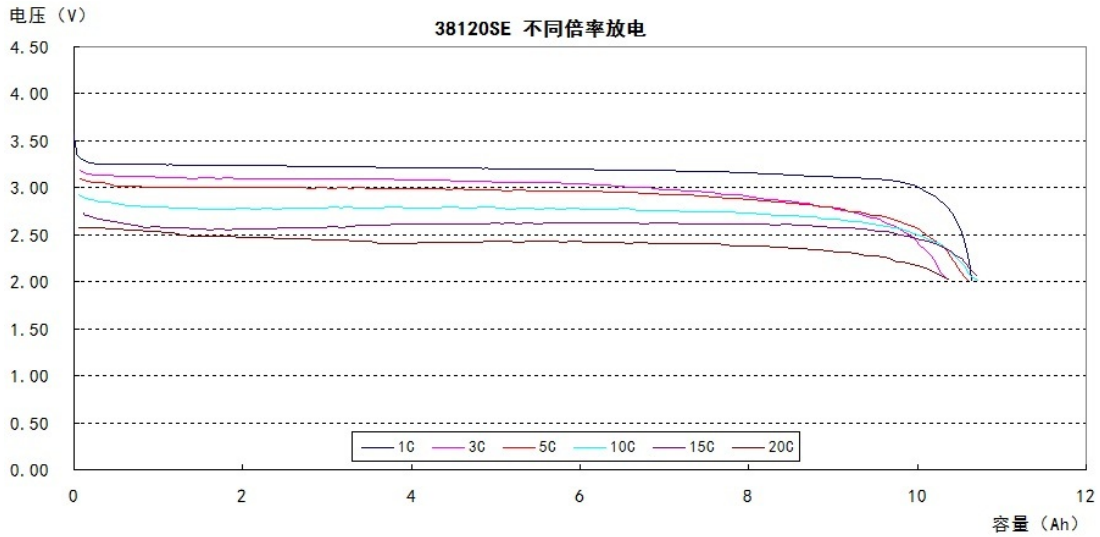

Figure 2.5 Battery discharge curve from HeadWay, "38120S 10Ah LiFePO4 Single Cell Specification Sheet," 38120S datasheet. [Online]. Available: http://www.headway-headquarters.com/38120s-10ah-headway-energy-cell/ [Accessed 2 February 2015]. Used under fair use, 2015.

2.2 Input Impedance of Different Converter Topologies

In order to extract maximum power from the energy harvester, the input impedance of the converter should be able to emulate a resistor. The following section discusses how the input impedance can be calculated for different commonly used power converter topologies operating in Continuous Conduction Mode (CCM) and Discontinuous Conduction Mode (DCM). CCM operation refers to a power converter whose inductor current is always greater than zero during a

switching cycle. Conversely, DCM operation refers to a power converter where the inductor current becomes zero during a certain period of a switching cycle. The crossover point between these modes is referred to as the critical boundary, and operating under this condition is referred to as boundary-conduction-mode (BCM). All of these operation conditions are illustrated in Figure 2.6. In general, DCM has lower switching conduction loss than CCM, resulting in higher efficiency if the converter operates in DCM [7].

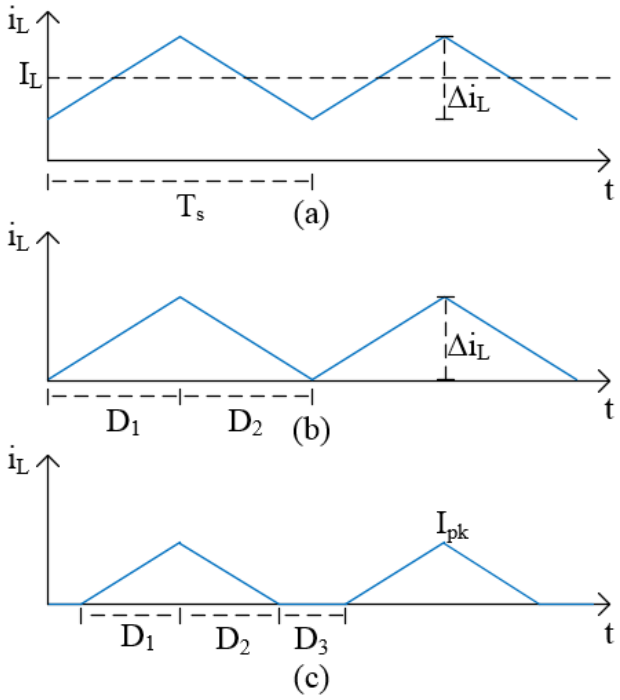

Figure 2.6 Inductor current waveforms (a) during CCM operation, (b) at the critical boundary, and (c) during DCM operation.

CCM and DCM operations affect the conversion ratio and the input impedance for all converter topologies. The steady-state input resistances are derived from circuit models obtained by averaging the waveforms within the circuits, as discussed in [8]. All conversion ratios and input impedance calculations were verified in this thesis research using Simplis to check for accuracy of the derived equations.

2.2.1 Buck Converter

The buck converter topology shown in Figure 2.7 converts a high input voltage down to a lower output voltage. The topology can be adopted to the target application when a battery with

a lower voltage is used instead of the current battery. It can also be used for a multi-stage approach to fulfill all the application requirements.

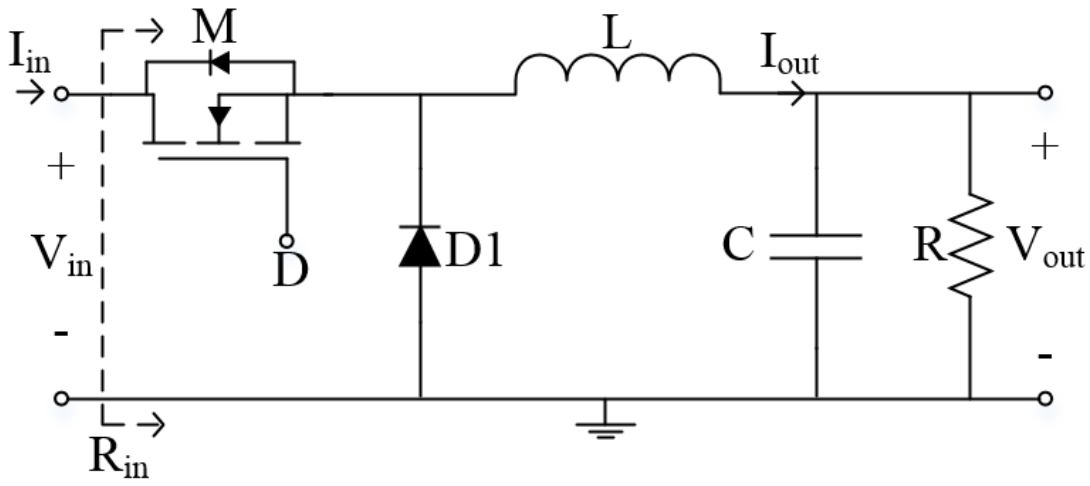

Figure 2.7 Buck converter circuit topology.

The conversion ratio for the buck converter operating in CCM is given in (2.2.1), and its derivation is available in [9].

$$\frac{V_{out}}{V_{in}} = D \tag{2.2.1}$$

The input current is equivalent to the transistor current in (2.2.2).

$$I_{in} = D * I_{out} \tag{2.2.2}$$

The average charge Q to the output capacitor, C, is zero in steady-state. Thus the output current is obtained in (2.2.3).

$$I_{out} = \frac{V_{out}}{R} \tag{2.2.3}$$

The input resistance for the buck converter operating in CCM can be obtained by combining (2.2.1)-(2.2.3) and is given in (2.2.4).

$$I_{in} = D\left(\frac{V_{out}}{R}\right) \rightarrow I_{in} = D\left(\frac{DV_{in}}{R}\right)$$

$$R_{in,buck,CCM} = \frac{V_{in}}{I_{in}} = \frac{R}{D^2} \tag{2.2.4}$$

(2.2.4) indicates that the average input resistance for the buck converter operating in CCM is dependent on the output resistance and the duty cycle only.

The input resistance for DCM operation of the buck converter can be obtained in a similar manner. The peak input current can be found by calculating the maximum inductor charging current during the D_1 cycle period of the switching cycle. This value can be averaged over the whole switching cycle to find the average input current and is given in (2.2.5).

$$I_{pk} = \frac{(V_{in} - V_{out})D_1 T_s}{L}$$

$$I_{in} = \frac{I_{pk} D_1}{2} = \frac{(V_{in} - V_{out})D_1^2 T_s}{2L} \tag{2.2.5}$$

The conversion ratio of the buck converter in DCM is derived in [9] and is shown in (2.2.6).

$$\frac{V_{out}}{V_{in}} = M = \frac{2}{1 + \sqrt{1 + \frac{8L}{D_1^2 R T_s}}} \tag{2.2.6}$$

Substituting the conversion ratio for the output voltage leads to the input resistance, which is given in Equation (2.2.7).

$$I_{in} = \frac{(V_{in} - MV_{in})D_1^2 T_s}{2L}$$

$$R_{in,buck,DCM} = \frac{V_{in}}{I_{in}} = \frac{2L}{(1-M)D_1^2 T_s} \quad where \;\; M = \frac{2}{1 + \sqrt{1 + \frac{8L}{D_1^2 R T_s}}} \tag{2.2.7}$$

Unlike CCM, the average input resistance in DCM is dependent on the inductance, switching frequency, duration of the on-period of the switching cycle, as well as the output resistance. The input resistance during DCM being dependent on the output resistance can cause difficulty in maintaining a constant input resistance since the input and output will have to be monitored closely to obtain the optimal duty cycle. In addition, buck converters are limited to the input voltage being larger than the output voltage, as discussed previously. Similar analysis of the buck converter operating in DCM and CCM can be found in [10], and the derived equations above were verified through simulation.

2.2.2 Boost Converter

The boost converter topology shown below in Figure 2.8 converts a low input voltage to a higher output voltage. This limits its application to scenarios where the output voltage is always higher than the input voltage.

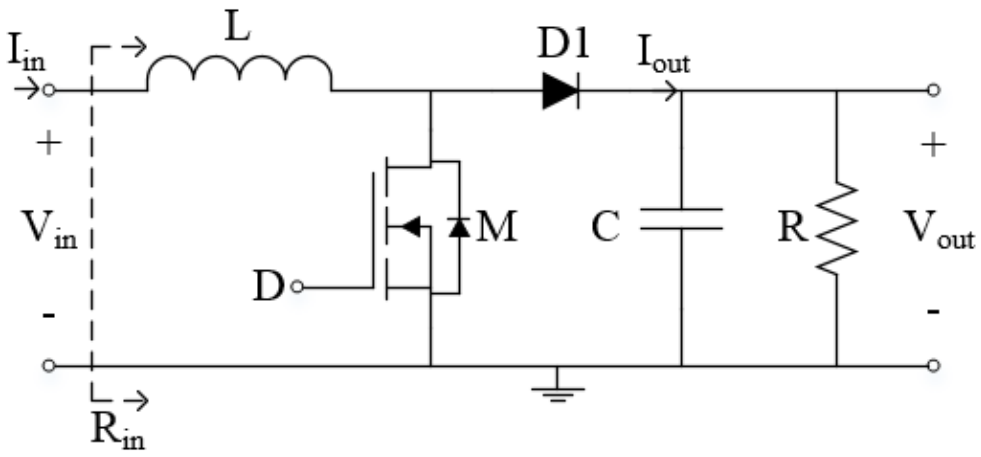

Figure 2.8 Boost converter circuit topology.

The conversion ratio for the boost converter operating in CCM, also derived in [9], is shown in (2.2.8).

$$\frac{V_{out}}{V_{in}} = \frac{1}{(1-D)} \tag{2.2.8}$$

The input current is equal to the inductor current, and the average inductor current is given in (2.2.9).

$$I_{in} = \frac{V_{out}}{R(1-D)} \tag{2.2.9}$$

Substituting (2.2.8) into (2.2.9), yields the input resistance shown in (2.2.10).

$$I_{in} = \frac{V_{in}}{R(1-D)^2}$$

$$R_{in,boost,CCM} = \frac{V_{in}}{I_{in}} = R(1-D)^2 \tag{2.2.10}$$

The input resistance to the boost converter operating in CCM depends on the output resistance and the duty cycle.

The input resistance of the boost converter in DCM operation is more complicated to calculate. The peak current through the inductor is given in (2.2.11).

$$I_{pk} = \frac{V_{in} D_1 T_s}{L} \tag{2.2.11}$$

The average inductor currents during the first part of the switching period, D_1, and the second part of the switching period, D_2, can be obtained using the peak inductor current and are shown in (2.2.12) and (2.2.13), respectively.

$$I_{inD_1} = \frac{V_{in} D_1^2 T_s}{2L} \tag{2.2.12}$$

$$I_{inD_2} = \frac{V_{in} D_1 D_2 T_s}{2L} \tag{2.2.13}$$

The average inductor current over a whole switching period can be obtained by adding both the individual averages. The resulting input resistance obtained from the average inductor current is given in (2.2.14).

$$I_{in} = \frac{V_{in} D_1 T_s}{2L}(D_1 + D_2)$$

$$R_{in,boost,DCM} = \frac{V_{in}}{I_{in}} = \frac{2L}{D_1 T_s (D_1 + D_2)} \tag{2.2.14}$$

The input resistance for DCM operation is dependent on the inductance, switching frequency, and both the charging and discharging stages of the switching cycle. The discharging stage of the switching cycle, D_2, can vary considerably depending on the input voltage, making the input resistance difficult to control in the target application. Furthermore, the boost converter is limited to having the output voltage higher than the input voltage. Similar analysis of the input resistance of a boost converter can be found in [11]. The conversion ratio and input resistance were verified through simulation.

2.2.3 Inverting Buck-Boost Converter

The buck-boost converter topology illustrated in Figure 2.9 is converts an input voltage to a higher or lower output voltage. Further, the polarity of the output voltage is flipped, essentially creating a negative output voltage, when referenced to the input voltage. However, this issue can be addressed by moving the diode D1 to the lower portion of the circuit topology and leaving the input voltage floating. This topic is discussed further in Section 3.3.2.

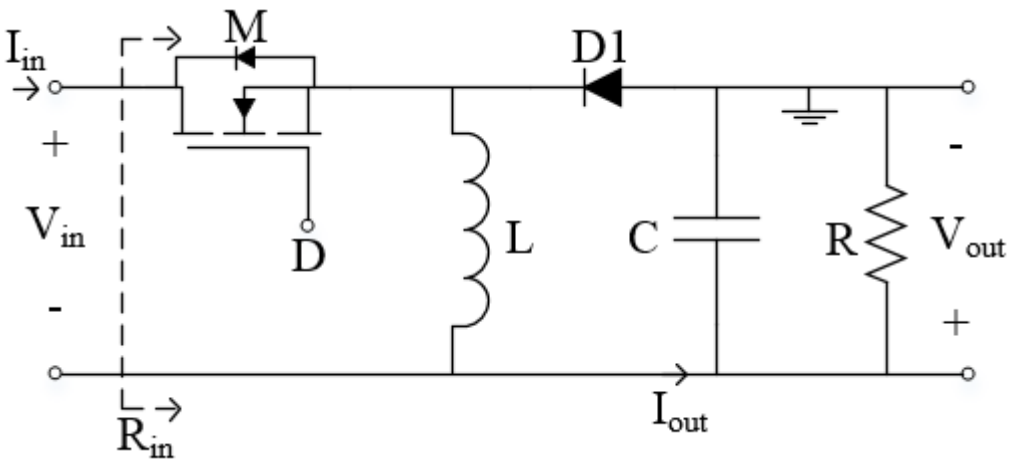

Figure 2.9 Buck-boost circuit topology.

The conversion ratio for the inverting buck-boost converter operating in CCM is derived in [9] and is reproduced below in (2.2.15).

$$\frac{V_{out}}{V_{in}} = -\frac{D}{(1-D)} \tag{2.2.15}$$

The average input current can be found by taking the average inductor current over the charging period of the switching cycle, as given in (2.2.16).

$$I_L = -\frac{V_{out}}{R}$$

$$I_{in} = -\frac{DV_{out}}{(1-D)R} \tag{2.2.16}$$

Combining (2.2.15) and (2.2.16) yields the input resistance for the buck-boost converter operating in CCM, shown in (2.2.17).

$$I_{in} = \frac{-D\left(-V_{in}\frac{D}{(1-D)}\right)}{(1-D)R}$$

$$R_{in,buck-boost,CCM} = \frac{V_{in}}{I_{in}} = \frac{R(1-D)^2}{D^2} \tag{2.2.17}$$

Similar to buck and boost converters operating in CCM, an inverting buck-boost converter operating in CCM depends on the output resistance and the duty cycle, D.

Derivation of the input resistance of the buck-boost converter in DCM can be achieved in a similar manner. The peak inductor current can be obtained as in (2.2.18).

$$I_{pk} = \frac{V_{in} D_1 T_s}{L} \tag{2.2.18}$$

The input current is equal to the average inductor current over the charging period of the switching cycle, D_1. The input resistance of the buck-boost converter operating in DCM is readily obtained after averaging the inductor current over the charging period, as shown in (2.2.19).

$$I_{in} = \frac{I_{pk} D_1}{2} = \frac{V_{in} D_1^2 T_s}{2L}$$

$$R_{in,buck-boost,DCM} = \frac{V_{in}}{I_{in}} = \frac{2L}{D_1^2 T_s} \tag{2.2.19}$$

The input resistance of a buck-boost operating in DCM is dependent on only the inductance, duty cycle, and switching frequency. These variables can easily be kept static to maintain a constant input impedance, independent of the input voltage level and output resistance. This property makes the inverting buck-boost topology attractive for applications requiring constant input impedance [12]. Since the buck-boost topology is capable of maintaining a constant input impedance and handling input voltages higher or lower than the output voltage, it is the most suitable converter for the target application.

2.3 Existing Converter Design Approaches for Vibration-Based Energy Harvesting

2.3.1 Cao's Approach for Mini Vibrational Power Generator

Cao proposed a small scale vibration energy harvester with a boost converter in which the output voltage of the generator is most often lower than the voltage of the storage element (Cao, Chiang, King, & Lee, March 2007). Cao implemented a combination feedforward and feedback control scheme in the hopes of improving efficiency by adjusting the duty cycle according to the input voltage [13]. The primary circuit elements found in Cao's converter design are shown in Figure 2.10.

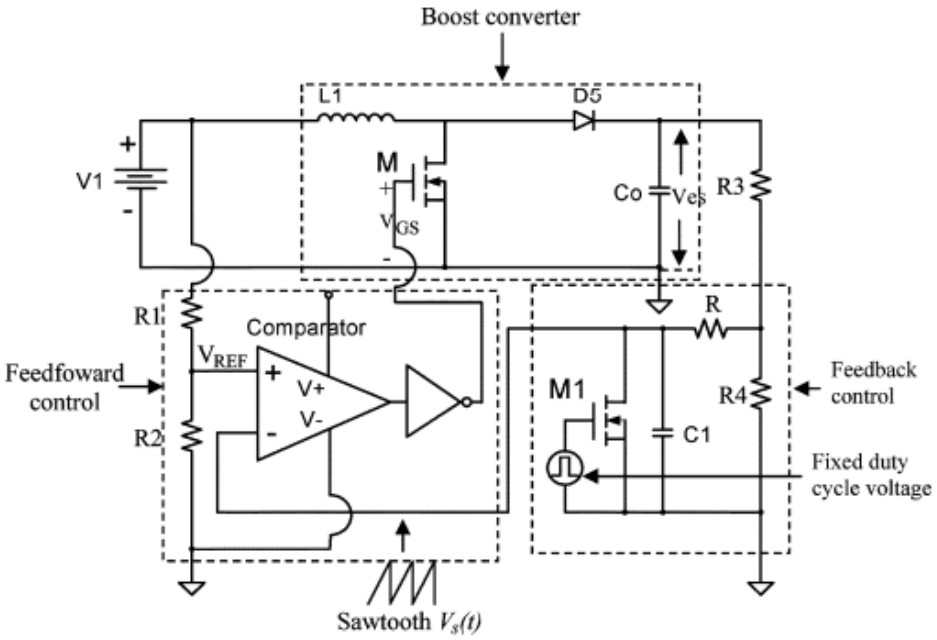

Figure 2.10 Circuit Schematic of feedforward and feedback boost converter from X. Cao, W.-J. Chiang, Y.-C. King and Y.-K. Lee, "Electromagnetic Energy Harvesting Circuit with Feedforward and Feedback DC-DC PWM Boost Converter for Vibration Power Generator System," Power Electronics, IEEE Transactions on, vol.22, no.2, pp.679,685, March 2007. Used under fair use, 2015.

Cao's design uses a super capacitor as the storage element and not a battery. This prevented the need for battery protection elements to be included within the control scheme. In addition, it allowed the output voltage information to be used more easily in the feedback network, since the voltage on a capacitor can change much more quickly than on a battery. The output voltage information is used to create a sawtooth waveform used with a comparator. The reference voltage to the comparator is derived from the input voltage information to determine the duty cycle. Cao's design also uses a diode to conduct input power to the output when the input voltage is higher than the output, since boost converters can only convert input voltages to higher output voltages. Cao's design does not include any mechanism in the control scheme to extract maximum power from the harvester. Finally, Cao does not explicitly state what sort of efficiency is achieved with this circuit or how it's performance affects the amount of power extracted from the harvester.

Nonetheless, Cao's approach to use feedforward and feedback voltage information to control the duty cycle is a very practical approach when designing power converters which must deal with a wide range of input voltages. This is the case with harvesting energy from vibration-

based ambient sources. Utilizing the input and output voltage information will be implemented in the proposed prototype, discussed in Section 3.4.

2.3.2 Dwari's Direct AC-to-DC Approach

Dwari et al. proposed a power converter for vibration-based energy harvesting, shown in Figure 2.11, whose major objective was to eliminate the diode rectification stage before the power converter [14]. The motivation behind this approach was rooted in the low voltages generated by electromagnetic micro-generators limited by size constraints. The circuit operates by conducting current in different directions depending on the input voltage polarity to achieve a single polarity output. Instead of a diode bridge rectifier, a bidirectional switch comprised of two MOSFETs is used. Dwari's proposed design does not require input polarity sensing, and the diodes D3 and D4 can be replaced with capacitors to further improve efficiency. Thus, the reported efficiency is fairly good, with efficiency of about 61% for the converter shown in Figure 2.11, and about 65% for the same type of converter but D3 and D4 are replaced with capacitors.

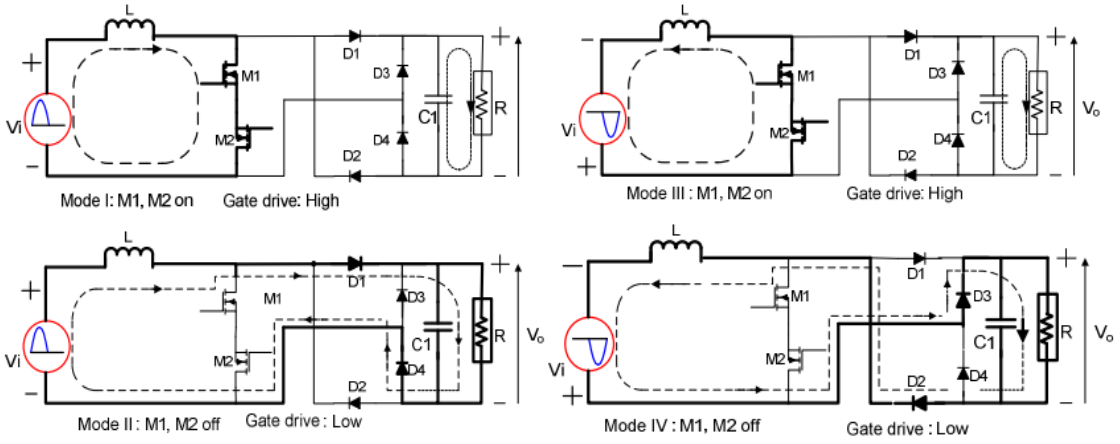

Figure 2.11 Circuit schematic and operating modes of direct AC-to-DC converter from S. Dwari, R. Dayal, P. Leila and K. N. Salama, "Efficient Direct AC-to-DC Converters for Vibration-Based Low Voltage Energy Harvesting," Industrial Electronics, 2008. IECON 2008. 34th Annual conference of IEEE, vol., no., pp.232-,2325, 10-13 Nov. 2008. Used under fair use, 2015.

Although Dwari et al.'s design achieves it's goal of eliminating the diode bridge rectification stage, it is not particularly applicable to an energy harvester for freight railcars for several reasons. First, the peak voltage considered for Dwari et al.'s converter is only 400 mV, whereas the voltage range for the freight railcar energy harvester, even after diode bridge

rectification, can be as high as 20 V. So elimination of a diode bridge rectifier is less significant for a freight railcar energy harvester. Second, the output of the RTL harvester is a 3-phase AC waveform, whereas Dwari's is designed only for a single phase, meaning significantly more components would need to be included in the power stage of a three-phase design. Third, Dwari's converter does not consider a battery load, only a resistive load, meaning no battery charging techniques are included in the control scheme. Finally, Dwari's design focuses primarily on high conversion efficiency, not maximum power extraction from the harvester. Thus, the net energy harvest is not necessarily high for the design.

2.3.3 Bandyopadhyay's Dual-Path Architecture Approach

Bandyopadhyay proposed a converter design that would be suitable for multiple different energy harvesting sources, including solar, thermal, and vibration [15]. The schematic diagram of the energy harvesting circuit proposed by Bandyopadhyay is shown in Figure 2.12. The dual-path architecture operates in one of three modes. If the harvested energy is available to support the load, the primary converter path is used to charge the capacitor at V_{load}. If more energy is harvested than is needed by the load, the secondary converter path is also used to transfer the excess energy to the capacitor at V_{store}. When there is not enough harvested energy to support the load via the primary path alone, a backup converter is used to convert the previously stored energy at V_{store} to help support the load. The converter for vibration-based energy harvesting sources uses a non-inverting buck-boost topology and the proposed dual-path architecture to achieve higher efficiency than a two-stage conversion approach and provide power to a current-sink load.

Bandyopadhyay's design is centered on supporting a load with a certain current consumption. Since there is no specified load for the target application other than the battery, there is no specified current consumption which needs to be sustained. Instead, the requirements for charging and protecting the life cycle of the battery are addressed in this application. Thus, a dual-path architecture may not be necessary, but may become applicable in future studies where a power consuming load is specified.

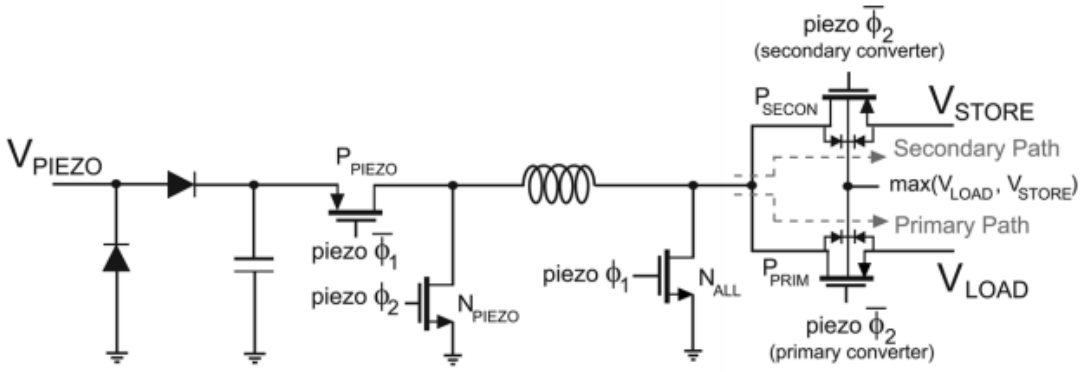

Figure 2.12 Circuit schematic of non-inverting buck-boost with dual-path architecture from S. Bandyopadhyay and A. Chandrakasan, "Platform Architecture for Solar, Thermal, and Vibration Energy Combining with MPPT and Single Inductor," *Solid-State Circuits, IEEE Journal of* , vol.47, no.9, pp.2199,2215, Sept. 2012. Used under fair use, 2015.

2.4 Battery Charging and Protection

2.4.1 Battery Charging Techniques

A battery charging circuit intends to prolong the life-cycle of a battery in the hopes of reducing operation maintenance costs. One of the most common battery charging approaches is called the constant current/constant voltage (CC/CV) technique. The CC/CV approach applies a constant current to the battery until the battery voltage reaches a predetermined level, indicating the battery is near fully charged. Then, the charge profile switches to maintain the charging voltage and reduce the charging current until the battery is fully charged and the charging current shuts off, as illustrated in Figure 2.13 [16].

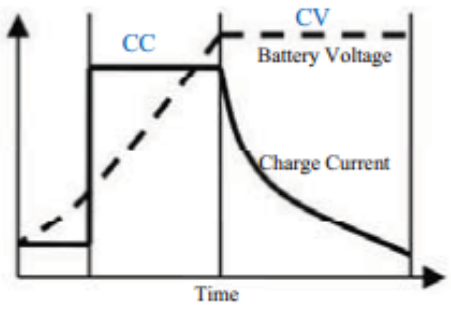

Figure 2.13 Constant current / constant voltage charging profile from X. Qu, H. Han, S.-C. Wong and C. Tse, "Hybrid IPT Topologies with Constant-Current or Constant-Voltage Output for Battery Charging Applications," *Power Electronics, IEEE Transactions on*, vol.PP,no.99,pp.1,2015. Used under fair use, 2015.

An improved charging technique considers more deeply the chemical process occurring within the battery and is referred to as pulse charging. This technique operates by providing a charging current to the battery, followed by a brief period of discharge or no charge [17]. The pulse charging technique allows ion concentration at the electrodes to disperse throughout the chemistry of the battery during charging, producing a more even gradient of ions between the electrodes. If the ions are allowed to concentrate at the electrodes, dendrites can form on the electrodes, resulting in a higher internal resistance, reduced capacity, and a shortened life cycle of the battery [18]. Fortunately, the sporadic nature of vibration-based energy harvesting already includes the potential for spikes in charging current and periods of time where the ions can disperse during low energy harvesting periods. Thus, the conditions of the target application already achieves a pseudo pulse-charging operation.

Amanor-Boadu et al. proposed a battery charger described in [19] which can handle inputs from multiple energy harvesting sources. The approach uses a supercapacitor to capture energy from the energy harvesters and the battery charger turns on once the voltage level of the supercapacitor reaches a predetermined voltage level. Their charging profile consists of a trickle charge mode, fast charging mode, and a slow charging mode as shown in Figure 2.14. Their primary charging modes use pulsed current charging and limit the charging current as the battery becomes ‘full’ in order to prolong battery life cycle. While the circuit lacks energy harvesting elements, the battery charging scheme has several merits. Switching between the charging modes to prolong battery life is adopted in the proposed control scheme.

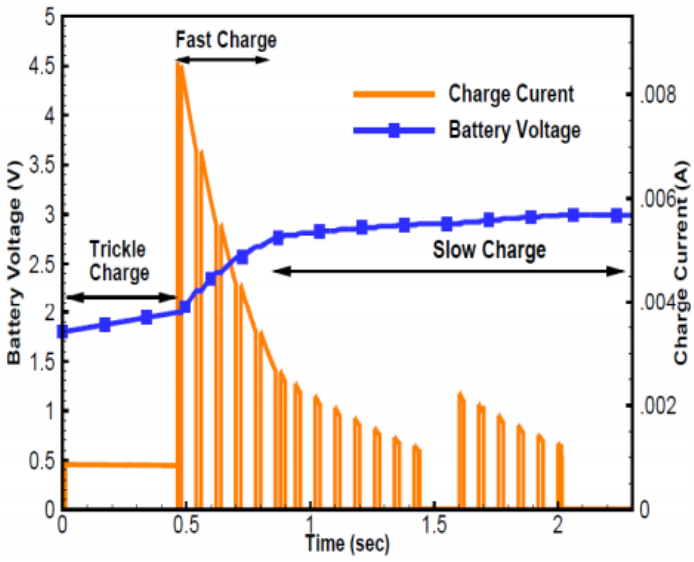

Figure 2.14 Charging profile based on battery voltage level proposed by J. Amanor-Boadu, M. Abouzied, S. Carreon-Bautista, R. Ribeiro, L. Xiaosen and E. Sanchez-Sinencio, "A Switched Mode Li-ion Battery Charger with Multiple Energy Harvesting Systems Simultaneously Used as Input Sources," *Circuits and Systems (MWSCAS), 2014 IEEE 57th International Midwest Symposium*, pp. 330,333, 3-6 Aug 2014. Used under fair use, 2015.

2.4.2 Control Schemes for Output Regulation Mode

Since the ambient energy harvested is sporadic, a simple way to control the output voltage is to sense the input voltage and adjust the duty cycle accordingly. It requires a fast change of the duty cycle according to input voltage changes. DCM operation is desired to reduce losses, as previously discussed in Section 2.2, which means the conversion ratio follows a nonlinear trend to be covered in Section 3.4.2. One-cycle control proposed by Smedley and Ćuk is a nonlinear control method used to control the duty cycle based on the input voltage magnitude [20], and it is illustrated for a buck converter in Figure 2.15. The control scheme is comprised of an integrator to monitor the input voltage, a comparator to compare the integrated input voltage to a reference voltage, and an RS flip-flop to control the duty cycle as well as provide a reset signal for the integrator. The nonlinear control scheme augments the duty cycle based on the comparison of a reference voltage with an integral of the input voltage. The one-cycle control (OCC) scheme can be adopted to implement the output regulation mode for the proposed converter. An implementation of the OCC for the proposed converter is covered in Section 3.4.2.

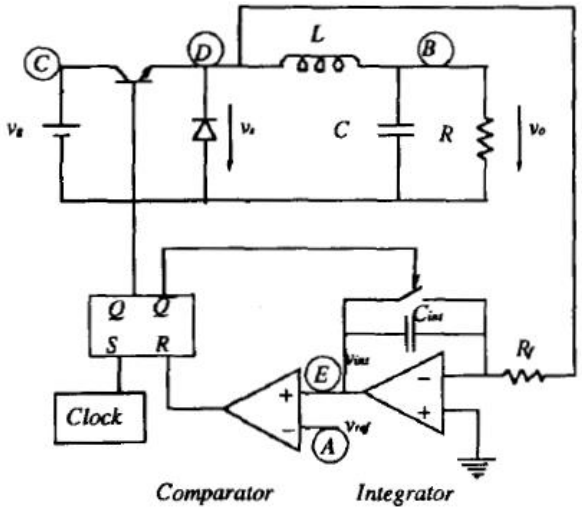

Figure 2.15 One-cycle control for buck converter from K. Smedley and S. Ćuk, "One-Cycle Control of Switching Converters," *Power Electrnoics Specialists Conference, 1991. PESC '91 Record, 22nd Annual IEEE*, vol. no. pp.888,896, 24-27 Jun 1991. Used under fair use, 2015.

A similar control scheme to one-cycle control is charge control. Although not used in this study, the charge control method is worth mentioning for its potential in future studies. Instead of integrating voltage, charge control integrates input current in order to control the duty cycle in a non-linear fashion [21]. The basic control scheme for charge control for a buck converter is illustrated in Figure 2.16. The input switch current is sensed and integrated by C_T while the switch is on. Once the voltage V_T on the integration capacitor C_T reaches the reference voltage V_C, the power stage switch is turned off and the voltage across the capacitor C_T is cleared with a switch. The operation principle of charge control is similar to one-cycle control, except input current information is used instead of voltage information. This control scheme may be useful in different applications.

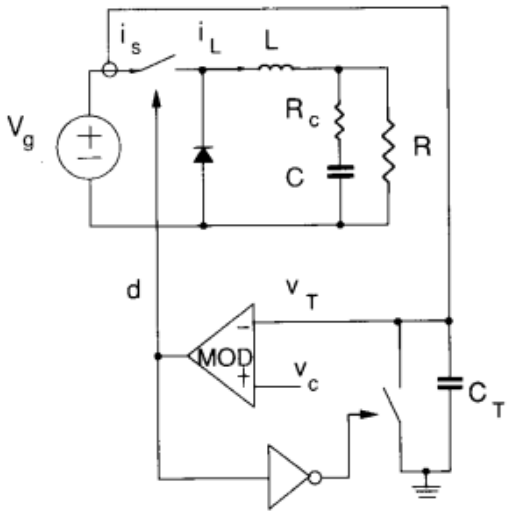

Figure 2.16 Charge control for buck converter from Tang, W.; Lee, F.C.; Ridley, R.B.; Cohen, I., "Charge control: modeling, analysis, and design," *Power Electronics, IEEE Transactions on*, vol.8, no.4, pp.396-403, Oct 1993. Used under fair use, 2015.

The proposed converter design includes battery charging techniques within the control scheme so the converter is not only designed for energy harvesting, but also for battery management. Fortunately, the sporadic nature of the ambient energy harvesting process already provides an inconsistent current to charge the battery, which follows along with the same principles as pulse charging battery schemes. A constant input impedance mode is used when the battery is not well charged, in order to extract maximum power from the harvester. When the battery is nearly fully charged, the proposed converter design switches over to an output regulation control mode. Finally, when the battery is fully charged, the converter shuts down to prevent overcharging of the battery. These three control modes will be referred to as constant impedance mode, output regulation (or one-cycle control) mode, and overvoltage shutdown mode throughout this thesis. The function of each mode is illustrated below in Figure 2.17.

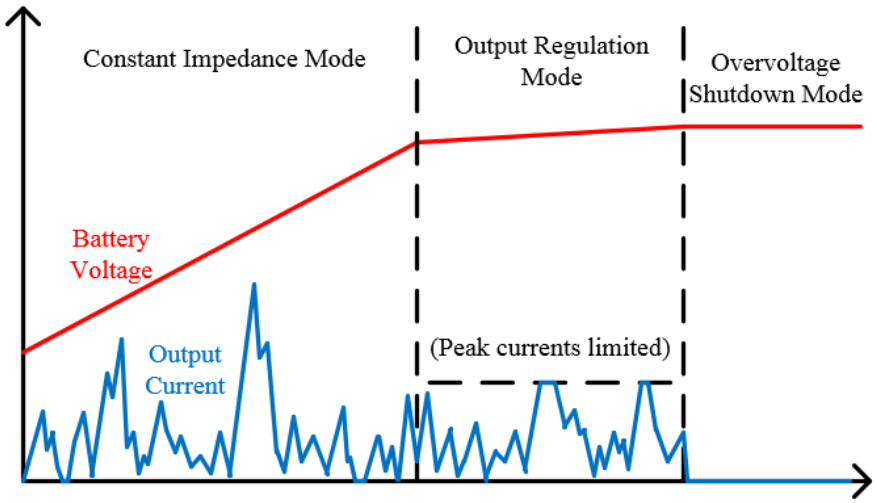

Figure 2.17 Proposed charging profile for new converter design.

2.5 Chapter Summary

This chapter begins by introducing the energy harvester developed for freight railcar applications. The energy harvester characteristics are used to define requirements of the proposed power converter. Related studies' previous approaches to power converter design for vibration-based energy harvesters as well as battery circuitry is discussed. Elements of the proposed design are derived from the approaches taken by previous studies and limited by the characteristics of the target application.

Chapter 3

Proposed Power Management Circuit: Control Scheme and Topology

The proposed power management circuit (PMC) for energy harvesting from freight railcars should satisfy several requirements imposed by the characteristics of the energy harvester and the battery pack. The first requirement is that the PMC should emulate a constant resistance for maximum power transfer when the battery voltage is below a threshold value. It is achieved by adopting the inverting buck-boost topology operating in DCM for the proposed circuit. The second requirement is that the PMC should protect the battery from overcharging. One-cycle control is adopted for the PMC to regulate the output voltage when the battery is close to fully charged. The third and final requirements is that the PMC should shut down when the battery is fully charged.

This chapter describes the design of the PMC to fit the above-mentioned requirements. To do so, the PMC operates in several different control modes. The operation of each of the control modes is covered in detail along with how the converter switches between the different control modes. Practical implementation of the converter is covered as well as a brief discussion on component selection.

3.1 Specifications

The target specifications of the proposed PMC are shown in Table 1. The rectified DC input voltage ranges 0-20 V, and the maximum output voltage is 12.8 V, set by the battery. When the battery voltage, $V_{Battery}$, is less than 11.5 V, or 90% of the battery charge, the PMC maintains a constant input resistance of 2 Ω, which extracts maximum power from the harvester. When $V_{Battery}$ ranges from 11.5 V to 12.8 V, (or between 90% and 100% of the battery charge), the PMC regulates the power converter output voltage to 13 V. When $V_{Battery}$ reaches 12.7 V, it is considered that the battery is fully charged. The PMC shuts down to block any further

charging current. The datasheet specifies a maximum charging current of the battery pack is 45 A [6] and the PMC current to the battery never exceeds this amount, given the considered input voltage range.

Table 1: Target Specifications for the Proposed PMC

Specification	Requirement
Input Voltage Range	0-20 V_{DC}
Maximum Output Voltage	12.8 V_{DC}
Constant Input Resistance Control Range	$V_{Battery}$ < 11.5 V (90% of Battery Charge)
Constant Voltage Control	11.5 V< $V_{Battery}$ < 12.8 V (Above 90% of Battery Charge)
Converter Shutdown	$V_{Battery}$ = 12.8 V% of Battery Charge

3.2 Block Diagram of the Proposed PMC

The proposed PMC is composed of an inverting buck-boost converter and a controller to emulate constant input resistance or regulate the output voltage depending on the battery voltage. Maximum power is extracted from the energy harvester when the harvester is presented with a constant load impedance of about 2 Ω, as shown in Section 2.1.1. As covered in Section 2.2.3, the input impedance of an inverting buck-boost converter operating in DCM is dependent on the power stage inductance, duty cycle, and switching period. The duty cycle and switching frequency can be set to constant values in order to achieve a constant input impedance to the converter. The duty cycle also controls the conversion ratio of the input voltage to the output voltage. This means it is not possible to maintain constant input resistance while regulating the output voltage. Hence, it is necessary to implement different operation modes for the converter: a constant input impedance mode, and an output voltage regulation mode, specifically through one-cycle control. The overvoltage shutdown control turns on if the battery reaches fully charged, as indicated by the output voltage level, and the converter shuts down with a 0% duty cycle. Adoption of different control modes intends to maximize the harvested energy while also protecting the battery life.

A block diagram of the proposed PMC is shown in Figure 3.1. The linear vibrations from the train suspension are mechanically translated into rotational energy, which spins a 3-phase AC electromagnetic generator [4]. The first stage of the converter is to rectify the 3-phase AC waveform into a DC voltage. Since the voltage and power levels of this application are much higher than typical vibration-based energy harvesting projects, rectification with low forward-voltage Schottky diodes is acceptable for the applciation, rather than taking a direct AC-to-DC conversion approach as in [14]. The power stage block is an inverting buck-boost converter comprised of a MOSFET, inductor, Schottky diode, and input/output capacitors. The battery load is made from four series-connected LiFePO4 batteries, each with ratings of 3.2 V and 10 Ah, resulting in a battery load rating of 12.8 V and 10 Ah. The actual battery voltage can be anywhere at or below 12.8 V, depending on charge level.

The controller actively monitors the battery voltage level to determine which control method to use: constant input impedance, output voltage regulation, or overvoltage shutdown. Logic gates and comparators are primarily used to determine which control method is used. The constant input impedance is maintained by keeping the duty cycle constant and operating the converter in DCM. The output regulation mode adopts one-cycle control to maintain the converter output voltage level by adjusting the duty cycle according to the input voltage level. Finally, if the battery becomes fully charged, the converter shuts down until the battery needs to be charged again to prevent overcharging the battery and to prolong battery life cycle. The controller design is the major part of this thesis research.

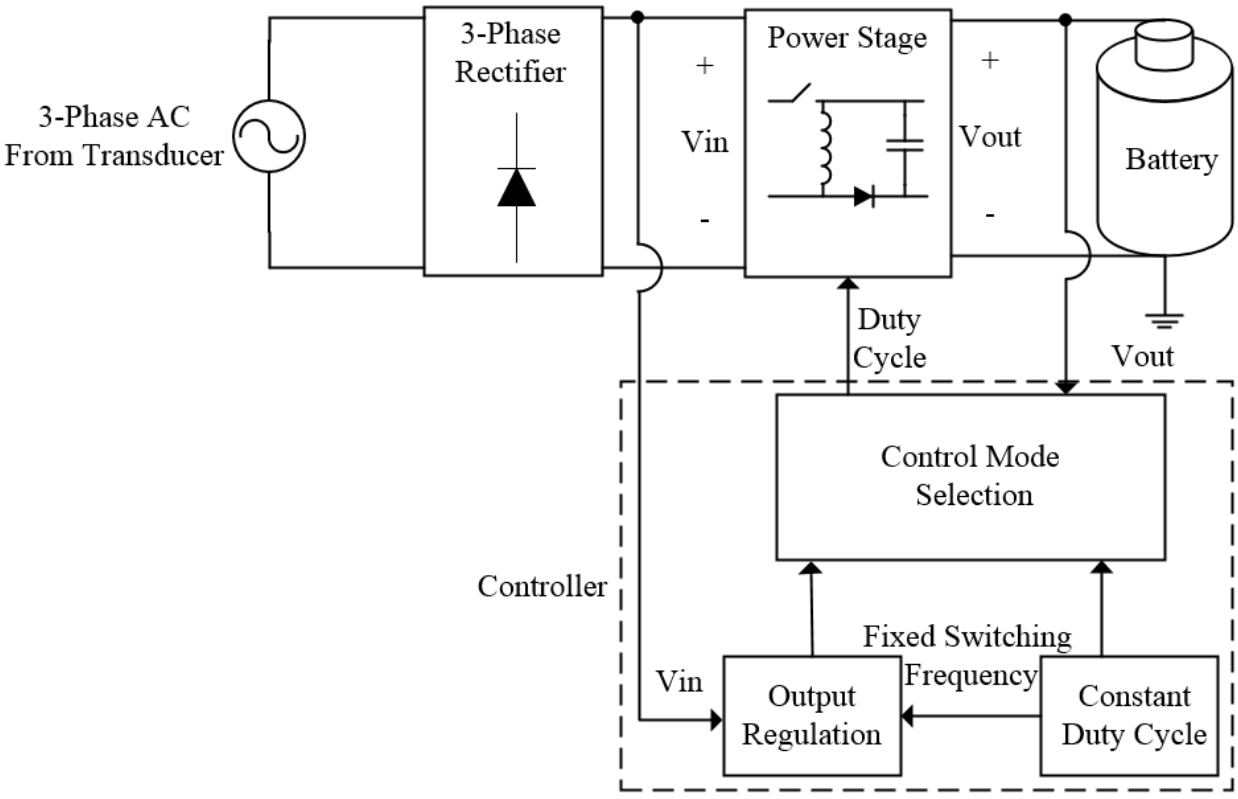

Figure 3.1 Block Diagram of Converter, Harvester, and Battery System.

3.3 The Bridge Rectifier and the Power Stage

3.3.1 Bridge Rectifier

The 3-phase rectifier below in Figure 3.2 is a typical 3-phase diode bridge rectifier, in which low forward-voltage Schottky diodes are used to minimize the amount of power lost. Specifically, the Schottky diodes are PMEG4050EP diodes, from NXP Semiconductor, which have a forward voltage of 490 mV at 5A. It is important to note that the power measurements shown in Section 2.1.1 were taken after the diode rectification bridge, which was constructed with diodes having a rated forward voltage of 850 mV at 5A. Thus, the power magnitude of the curves shown in Figure 2.2 should be slightly higher with these new diodes. More energy is already being extracted from the harvester by using better Schottky diodes in the rectification stage.

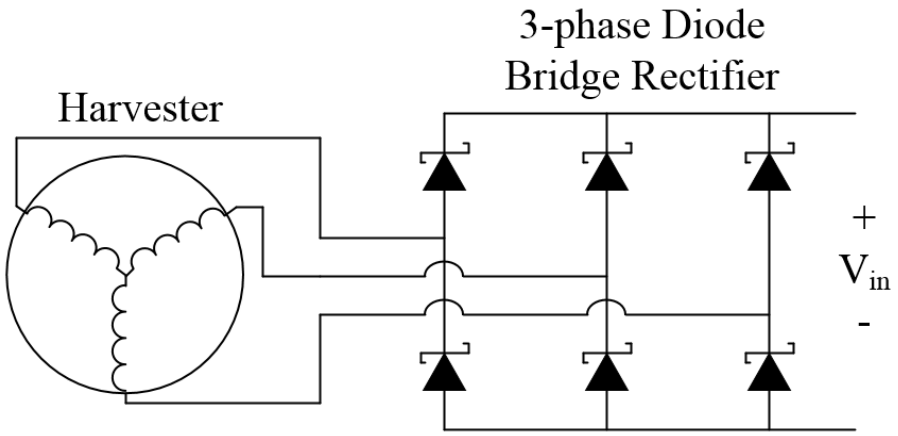

Figure 3.2 3-phase diode bridge rectification circuit diagram.

3.3.2 Power Stage

The power stage is an inverting buck-boost converter operating in DCM and is shown in Figure 3.3. The power stage consists of an output capacitor, Schottky diode, inductor, N-channel MOSFET, and an input capacitor that smooths out the voltage waveform from the diode bridge rectifier. The ground is the negative terminal of the battery, and the input voltage is left floating. This is because the discrete components used to make the controller must draw power from the battery, since the input power is sporadic and unreliable.

A low forward-voltage Schottky diode (D1) is used instead of a synchronous rectifier for the following reasons. If an N-channel MOSFET is used, the battery voltage would cause the reverse body diode of the N-channel MOSFET to conduct, resulting in reverse inductor current and CCM operation. A P-channel MOSFET can be used, but design of the gate driver is complex. This is due to the fact that commercial gate drivers which can handle both high-side N-channel MOSFETs and low-side P-channel MOSFETS simultaneously are not readily available. Individual gate drivers are available for N- and P-channel MOSFETS, but synchronicity between the two MOSFETs and incorporating dead time into the gate driving signals complicates the design. In addition to these requirements, the inductor current information would also need to be sensed in order to shut down the synchronous rectifier when the inductor current reaches zero. A synchronous rectifier could be a viable option for ICs, but it is out of the scope of this research.

The power stage was designed to be able to handle the maximum expected power from the energy harvester when it is stimulated by real-world track vibrations. The harvester has been proven capable of generating power in the order of hundreds of watts, but only with lab-based testing using unrealistic vibration displacement values. Considering a realistic amount of peak output power from the harvester allows lower voltage components to be used in the power stage, resulting in a more efficient converter.

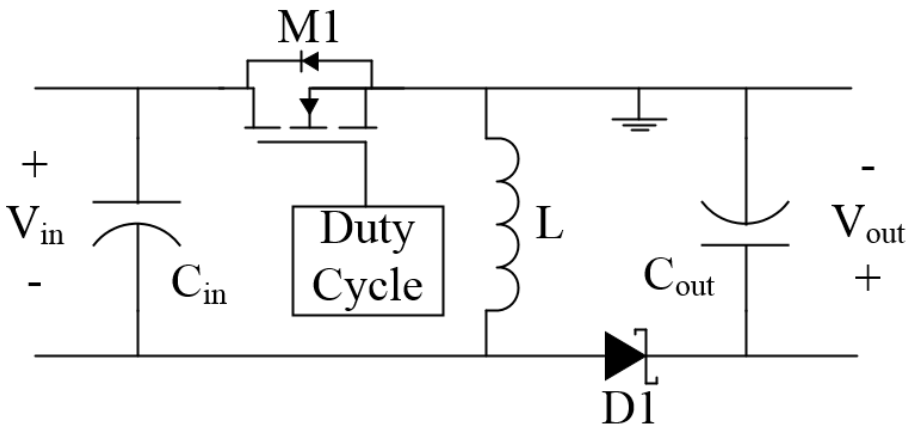

Figure 3.3 Inverting buck-boost power stage.

The current conduction waveforms of the inverting buck-boost converter operating in DCM and are illustrated in Figure 3.4. The current conduction paths of the inverting buck-boost converter operating in DCM in the context of the circuit diagram are illustrated in Figure 3.5. During Phase 1, the MOSFET is turned on, allowing current from the input source to flow, charging the inductor as shown in Figure 3.5 (a). During Phase 2, the MOSFET turns off and the energy stored in the inductor flows through the diode to supply the load and the output capacitor; this is shown in Figure 3.5 (b). Phase 3 occurs when the inductor current reaches zero and the load is supported by only the output capacitor until the next switching cycle occurs; this is shown in Figure 3.5 (c). It is important to note that when the inductor is discharging, the diode provides the only path for the current to flow. This is how the battery can be charged with current even when the duty cycle does not provide a higher output voltage than the battery voltage.

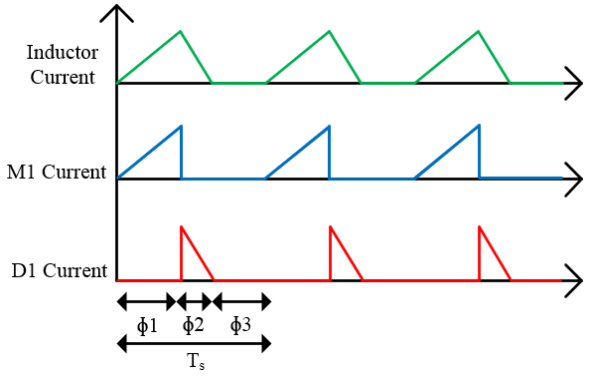

Figure 3.4 Current flow waveforms for power stage of buck-boost converter operating in DCM.

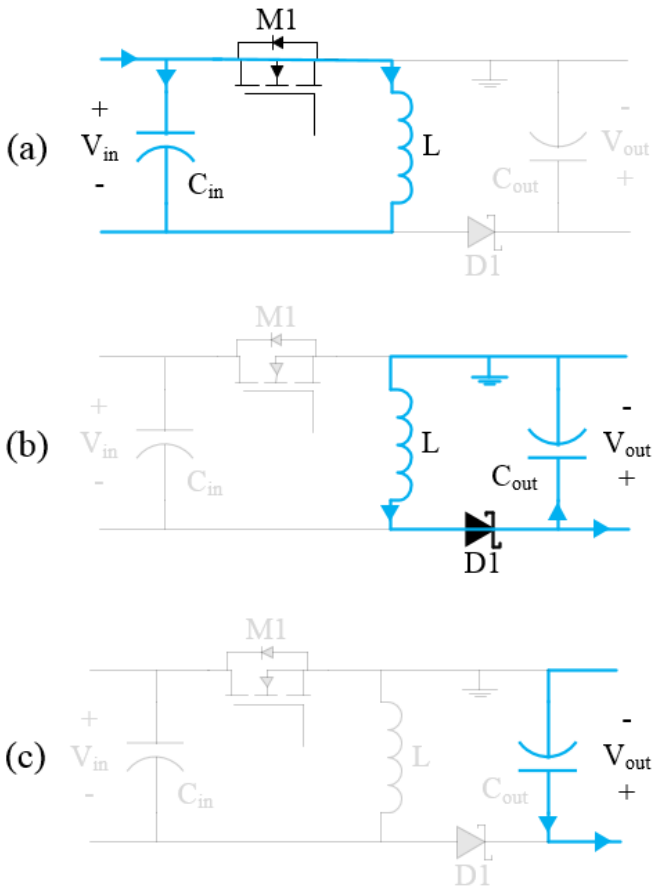

Figure 3.5 Current conduction phases for DCM during (a) Phase 1, (b) Phase 2, and (c) Phase 3.

3.4 Controller

The proposed converter has three control modes: constant input impedance, output regulation, and overvoltage shutdown. The following section explains the implementation of each control mode and the mode selector to select the appropriate control mode.

3.4.1 Constant Input Impedance Mode

The implementation of the constant input impedance mode is straightforward, since the duty cycle is fixed. A Texas Instruments (TI) LMC555 chip is used with two 10 kΩ potentiometers to generate a 30% duty cycle, 50 kHz square wave signal to act as the constant duty cycle for this control mode. The chip is operated in the astable operating mode as described in [22]. This signal is applied to the mode selector before being fed to the gate driver and to an MSMV which is used to generate the Reset signal for one-cycle control.

3.4.2 Output Regulation Mode

The output regulation mode regulates the output voltage to charge the battery using one-cycle control. The fluctuating input necessitates feedforward control to adjust the duty cycle accordingly. The conversion ratio for the inverting buck-boost converter operating in DCM is and is derived in [9] and given in (3.4.1).

$$\frac{V_{out}}{V_{in}} = D\sqrt{\frac{R_{out}T_s}{2L}} \tag{3.4.1}$$

The output voltage is dependent on the input voltage, the duty cycle, and the output resistance, assuming the switching frequency and inductance are constants. The output resistance, or the internal battery resistance was determined by measuring the internal resistance of the battery using the DC load method as described in [23]. This method consists of measuring the open circuit voltage of the battery, measuring the resistively-loaded battery voltage, and then calculating the battery internal resistance using the current through the resistive load and the difference between open-circuit voltage and loaded voltage. The results show a fairly consistent internal resistance over a range of different battery voltage levels in the operating voltage region for the proposed control method and are tabulated in Table 2.

Table 2: Battery internal resistance measurements.

V_{oc} (V)	V_{load} (V)	I (mA)	R_{int} (Ω)
12.501	12.491	0.843	11.86
12.476	12.466	0.841	11.89
12.436	12.426	0.838	11.93
12.426	12.416	0.837	11.95
12.412	12.402	0.836	11.96
12.363	12.354	0.833	10.80
12.285	12.276	0.828	10.87
		Average:	11.61

Since the battery internal resistance remains roughly constant, the duty cycle is now a function of the input voltage only. The appropriate duty cycle used to regulate the output voltage to 13 V for the range of considered input voltages is achieved for the following parameters and shown in Figure 3.6:

$$\frac{V_{out}}{V_{in}} = D\sqrt{\frac{R_{out}T_s}{2L}}, \qquad V_{out} = 13\ V, \qquad R_{out} = 11.6\ \Omega, \qquad T_s = 20\ \mu s, \qquad L = 1.8\ \mu H$$

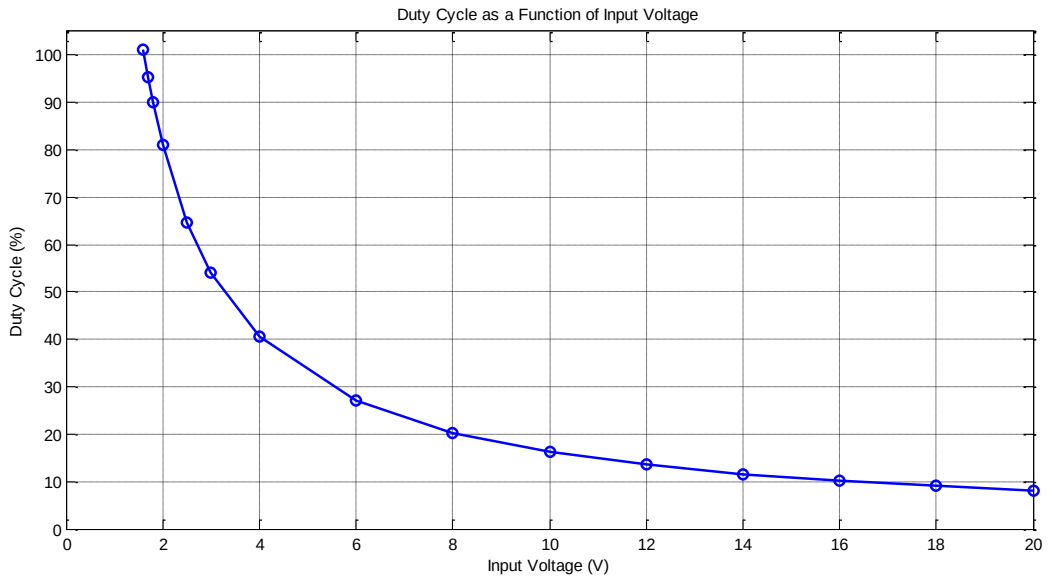

Figure 3.6 Duty cycle versus the input voltage used for regulating the output voltage to 13 V.

Figure 3.6 indicates several important characteristics that must be incorporated in the control scheme. First, the conversion ratio is nonlinear. Therefore, the control scheme must incorporate the nonlinear characteristic when determining the duty cycle. Second, the optimal

duty cycle is not feasible for low input voltages. This is apparent with the duty cycle going above 100% at input voltage levels below ~1.7 V. So, the constant input impedance control will take over for the proposed design if the input voltage is below a certain threshold (~1.8 V was chosen for this application). A much lower duty cycle or conversion rate than the optimal one should not cause any damage to the battery, while still allowing low input voltages to slowly charge the battery.

One-cycle control discussed in Section 2.4.2, is adopted for the proposed controller. Figure 3.7 shows the circuit diagram used to implement the one-cycle control scheme. As stated in section 3.3.2, the input voltage is floating in comparison to the ground reference which necessitates a differential voltage amplifier to sense the input voltage. A non-inverting differential voltage amplifier, which uses an LT1366 operational amplifier, senses the input voltage with a scale factor of four. This ensures that the input voltage is never outside of the battery-sourced supply rails provided to the op-amp, guaranteeing accurate tracking of the input voltage. The division ratio of the differential amplifier is related to the ratio of R_{d1} & R_{d2} to R_{d3} & R_{d4} as explained in [24] and is given below in (3.4.2).

$$\frac{V_{out-Diff\ Amp}}{V_{in}} = \frac{R_{d3}}{R_{d1}} \quad if \quad R_{d1} = R_{d2} \ \ \& \ R_{d3} = R_{d4} \qquad (3.4.2)$$

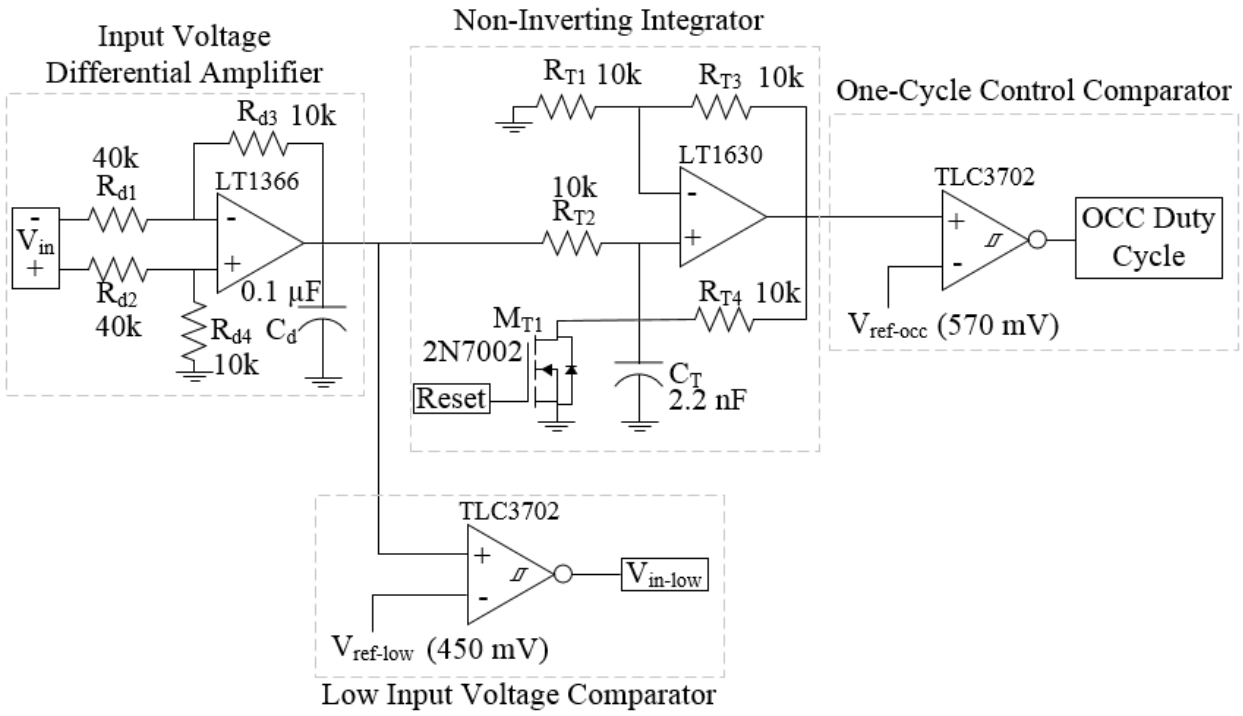

Figure 3.7 Circuit elements necessary for implementing One-Cycle Control in power converter.

The scaled input voltage is applied to the non-inverting integrator and the low input voltage comparator. The low input voltage comparator compares the scaled input voltage with the reference voltage, and sets its output signal, $V_{in\text{-}low}$, high if the input voltage is lower than the threshold voltage of ~1.8 V.

The non-inverting integrator is the heart of the control scheme. The integrator translates the magnitude of the input voltage into a voltage ramp from the capacitor being charged by the input voltage. The slope of the capacitor voltage ramp is proportional to the magnitude of the input voltage. The switching period is maintained by the MOSFET labelled M_{T1} and the gate driving signal labelled "Reset" in Figure 3.7. The 'Reset' signal is generated by a monostable multivibrator (MSMV) chip. The MSMV receives the constant duty-cycle signal from the LMC555 in order to have the appropriate 50 kHz switching frequency, and is then tuned to output a one-shot signal of only 1.5 µs in width. This corresponds to a 'Reset' signal that discharges the integrator capacitor during 7.5% of the switching period. The functionality of the non-inverting integrator circuit is discussed in further detail in [25].

The input-voltage-proportional ramp signal generated by the integrator block is then passed to the one-cycle control comparator, which determines an appropriate duty cycle based on

the input voltage ramp signal. The higher the input voltage, the steeper the ramp, and the quicker the ramp voltage reaches the compared voltage, resulting in a shorter duty cycle. The reverse is also true, where a lower input voltage produces a shallower integrator ramp, resulting in a longer duty cycle. Waveforms of the one-cycle control are illustrated in Figure 3.8. This trend follows closely with the curve represented in Figure 3.6, where higher input voltages results in lower duty cycles. The values of $R_{T1\text{-}T4}$ and C_T can be adjusted along with the $V_{ref\text{-}occ}$ reference voltage to generate the desired duty cycle corresponding to input voltage magnitudes.

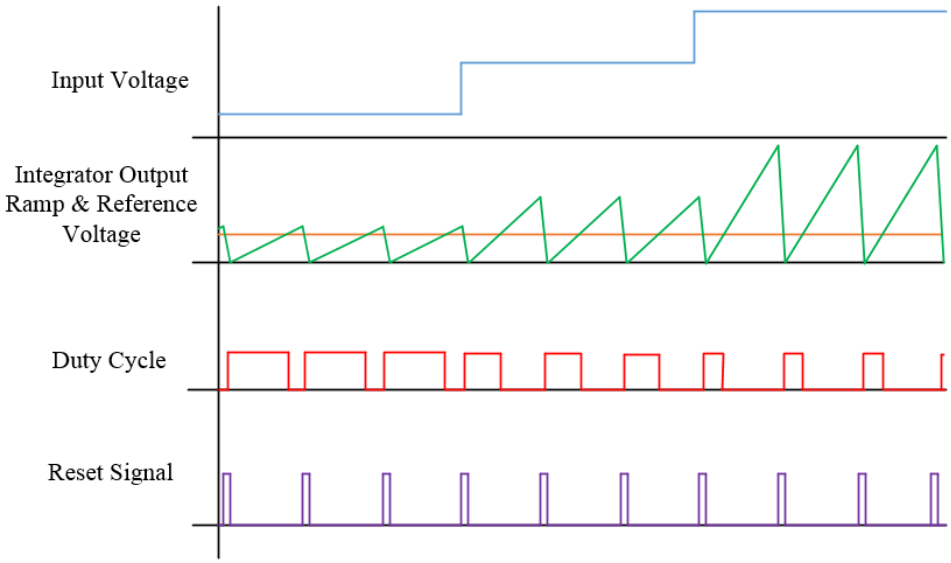

Figure 3.8 Waveforms of the one-cycle control.

3.4.3 Reference Voltage Generation and Mode Selector

The reference voltages and signals implemented by using the LT1236-5 are illustrated in Figure 3.9. The LT1236-5 precision reference chip is selected to provide a 5 V reference voltage, which is used to generate the reference voltages for the one-cycle control reference, $V_{ref\text{-}occ}$, and the low input voltage reference, $V_{ref\text{-}low}$. The one-cycle control reference "OCC Enable" becomes high if the battery voltage reaches 90% of the fully charged voltage, 11.5 V. The "Overvoltage Shutdown" reference signal becomes high once the battery voltage reaches 100%, or 12.8 V.

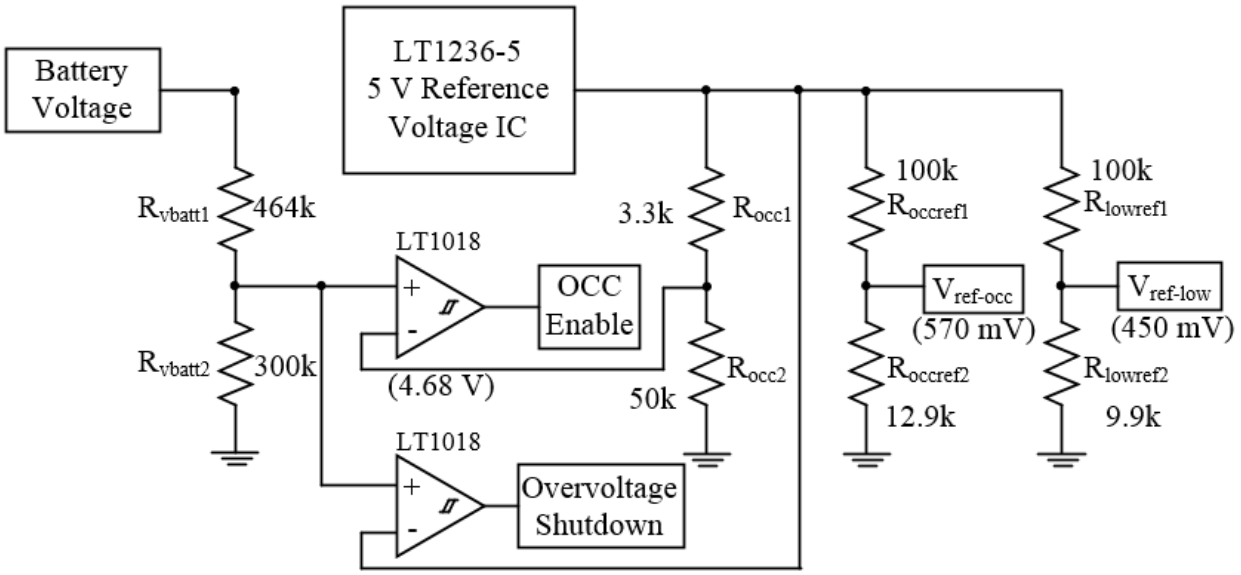

Figure 3.9 Circuitry used to generate reference voltages for comparators and logic gates.

The mode selector shown in Figure 3.10 selects an appropriate control mode based on the battery voltage, which is implemented by using three inverters, two AND gates, and two OR gates.

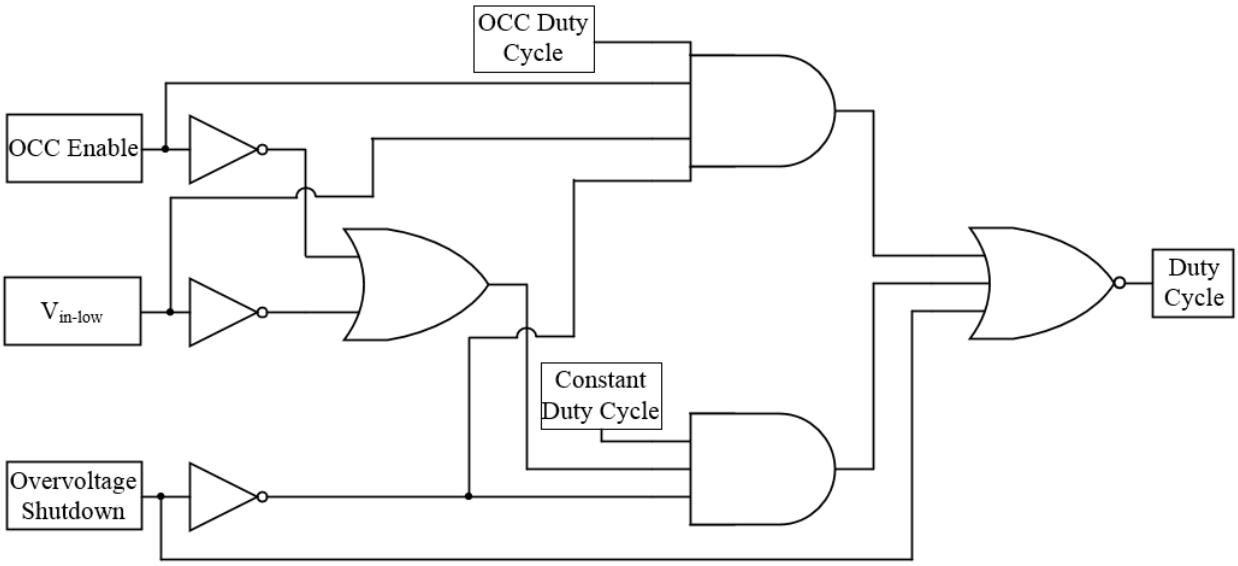

Figure 3.10 Logic network used to select between control schemes.

The truth table of the mode selector is shown in Table 3: Truth table for operation of mode selector.. The One-Cycle control mode is enabled if the battery voltage is between 90-100% (given by the OCC Enable and Overvoltage Shutdown signals) and if the battery voltage is high enough (given by the Vin-low signal). The constant duty cycle mode is enabled if the battery

voltage is below 90% (given by the inverse of the OCC Enable signal) or if the battery voltage is too low to support one-cycle control (given by the inverse of the Vin-low signal).

Table 3: Truth table for operation of mode selector.

Control Mode	OCC Enable	$V_{in\text{-}low}$	Overvoltage Shutdown	Duty cycle
Constant Impedance	1	0	0	Constant Duty Cycle
Constant Impedance	0	1	0	Constant Duty Cycle
One-Cycle Control	1	1	0	OCC Duty Cycle
Shutdown	x	x	1	None

3.5 Component Design and Selection

All components and circuitry used in the design of this power converter had to fit the application of having a single positive voltage power supply with a varying magnitude and wide input voltage range. The power stage components were selected based primarily on their potential to minimize conduction losses within the power stage. Components used in the implementation of the control network were selected to minimize quiescent power consumption while maintaining functionality throughout a wide range of possible supply voltages. A complete list of all the parts used to construct the final prototype can be found in Appendix B.

3.5.1 Power Stage Component Selection

The components of the power stage were selected primarily to minimize conduction losses and maintain DCM operation. The size of the input capacitor was selected to be large in order to compensate for the large fluctuation of input voltage magnitudes, resulting in a smoother input voltage. It is the same for the output capacitor. Low Equivalent Series Resistance (ESR) is also desirable for the capacitors in order to reduce losses from the capacitors. However, Capacitors with low ESR have a tradeoff between capacitance and maximum voltage rating. A maximum input voltage of 20 V allows low-ESR capacitors to be used at the input while maintaining high enough capacitance to reduce the input voltage ripple. Aluminum polymer OS-CON caps were selected for the input and output capacitors. Specifically, five EEH-ZA1V271P

capacitors with ratings of 270 μF, 20 mΩ, and 35 V were used for the input capacitor bank, totaling 1350 μF. Three PCR1D681MCL1GS capacitors with ratings of 680 μF, 14 mΩ, and 25 V were used for the output capacitor bank, totaling 2040 μF.

The switching frequency was chosen to be low, only 50 kHz, due to a number of desirable factors. Higher switching frequencies generally allow smaller components and allow for improved transient performance, but suffer larger switching losses. There is no strict requirement on the size of the converter, so size is not a concern. The voltage oscillations shown from typical load testing performed on the harvester (shown in Section 2.1.1) indicated very low frequency variations, not higher than 10 Hz, so very fast transient performance is not a large concern either. Reducing the conduction losses is desirable, and so a low switching frequency is chosen. A more detailed discussion on the general tradeoff between high and low switching frequencies is discussed in [26].

The inductor was chosen based on available inductors with low ESR to minimize conduction loss, high current saturation to handle large input voltages, and appropriate inductance to maintain DCM operation. Typically, the inductor current ripple is used to determine the appropriate size of the inductor, as in [9]. However, the main requirement for this application is that the converter maintains DCM operation even when subjected to the largest possible input voltage during the constant impedance control mode. Simulations were used to ensure that the converter stayed within DCM operation with differently sized inductors. The simulations indicated that a 2 μH inductor would be sufficient for maintaining DCM. The IHLP6767GZER1R8M01 inductor was chosen, which has inductance of 1.8 μH, saturation current rating of 65 A, and DC resistance of 2.1 mΩ.

The semiconductors used in the power stage were selected on a priority of having low conduction losses. The synchronous Schottky diode used for D1 is an STPS30L30DJF-TR. This Schottky diode has the best characteristics of the diodes surveyed, with a typical forward voltage range of only 0.3 – 0.45 V, blocking voltage of 30 V, and forward current rating of 45 A.

A MOSFET for a buck-boost converter should have a breakdown voltage rating of twice the voltage it will be subjected to. Since the maximum input voltage being considered is 20 V, the MOSFET breakdown voltage rating should be around 40 V. A brief survey of off-the-shelf MOSFETs yielded two candidates for this application. To aid in choosing the most suitable

device for this application, the Figure of Merit (FOM) of each MOSFET is evaluated. (3.5.1) shows the formula for FOM, which is a multiplication of the MOSFET's on-resistance ($R_{DS\text{-}on}$) and the gate charge (Q_g) characteristics [27].

$$FOM = R_{DS-on} \cdot Q_g \tag{3.5.1}$$

The two MOSFETs considered for this application are listed below in Table 4 with their respective characteristics and FOM.

Table 4: Typical characteristics from surveyed MOSFETS [28] [29]

Device	V_{BR}	Q_{gd}	C_{oss}	$R_{DS\text{-}on}$ (@10 V)	Q_g (@10 V)	FOM
IRFS7434	40 V	66 nC	1540 pF	0.7 mΩ	210 nC	147 mΩ·nC
CSD18509Q5B	40 V	17 nC	821 pF	1 mΩ	150 nC	150 mΩ·nC

Low FOM is a general characteristic useful for narrowing down the search for appropriate MOSFET candidates, but a loss breakdown over the application's range of operating conditions is necessary to select the lowest loss device. The three primary sources of MOSFET device losses in this application are conduction loss, gate driving loss, and switching loss. The primary concern of this application is the conduction loss, since the switching frequency is low. Conduction loss is a result of current being conducted from the drain to the source of the MOSFET. Since the output voltage level of the harvester is typically low under real-world displacement conditions, conduction losses are low most of the time, but can grow quite large under peak harvesting conditions. The conduction loss is a product of the on-resistance and the square of the conducted current, as shown in (3.5.2) [27].

$$P_{cond} = I_{in}^2 \cdot R_{DS-on} \tag{3.5.2}$$

Gate driving loss is the power dissipated during the charging and discharging cycle of the gate of the MOSFET when the device is turned on and off. The gate driving loss is dependent on the gate to source voltage, V_{gs}, applied by the gate driver, the total gate charge, Q_g, and the switching frequency, f_s. Thus, gate driving losses can be reduced by selecting a device with a lower gate charge characteristic. The equation used for calculating the gate driving loss is shown in (3.5.3) [27].

$$P_{gd} = V_{gs} \cdot Q_g \cdot f_s \tag{3.5.3}$$

The last source of loss considered for this application is the switching loss. Switching loss is the power dissipated for charging and discharging the parasitic capacitances associated with the MOSFET. The switching loss is a bit more complicated to calculate, since it is dependent on the time a device takes to turn on and off, which is related to several device-specific parameters. The commonly used equations for estimating the switching loss of a power MOSFET is shown below in (3.5.4) [30].

$$P_{sw} = \frac{I_{in} \cdot V_s \cdot (t_{off} + t_{on}) \cdot f_s}{2} + \frac{C_{oss} \cdot V_s^2 \cdot f_s}{2} \tag{3.5.4}$$

In order to properly compare the devices considered for this application, it is necessary to consider the performance of each device under low energy harvesting conditions and under peak conditions. The calculations can be simplified by assuming an average value of current for the given energy harvesting condition, which means the calculations correspond primarily to the constant input impedance mode of operation for the converter. Also, to match data given by tested operating conditions on the datasheets for these devices, V_{gs} and V_s are both assumed to be 10 V. The current conduction for light energy harvesting is 1 A and the peak conduction current is 7.5 A which correspond to input voltage levels of 2 V and 15 V, respectively, for a 2 Ω input impedance. The power loss breakdown for each device under light and peak harvesting conditions, is illustrated in Figure 3.11 and Figure 3.12, respectively.

Since the components were selected to minimize conduction losses, the primary source of loss in the light harvesting condition is gate driving loss. Under peak harvesting conditions, the primary source of loss is the switching loss. These figures also indicate a first order estimation of the power loss due to the physical characteristics of the selected MOSFET device. Since both devices were selected to minimize their conduction losses, the gate driving and switching losses contribute the largest amount of loss. Since the CSD18509Q5B has considerably lower output capacitance and gate charge characteristics, it produces less switching and gate driving losses than the IRFS7434. Although the IRFS7434 has a lower FOM, this analysis concludes that the CSD18509Q5B results in a slightly higher efficiency converter. Since these calculations were made with ideal equations and device parameters, both devices were included in the prototype design to evaluate the real-world performance of each device.

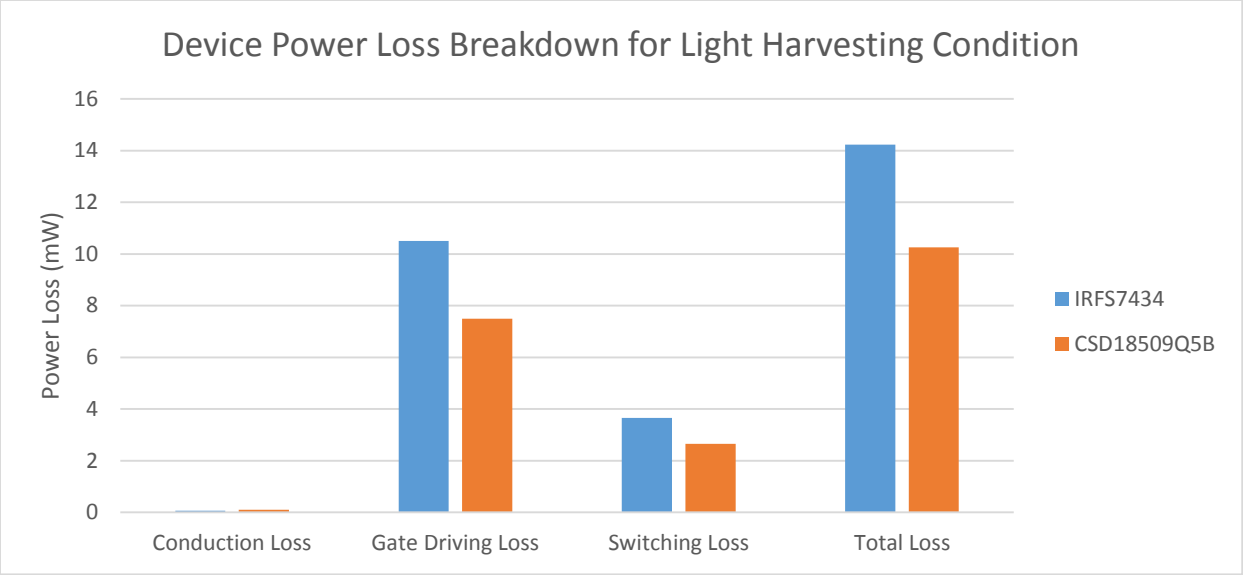

Figure 3.11 Power loss breakdown under light harvesting condition (V_{in} = 5 V).

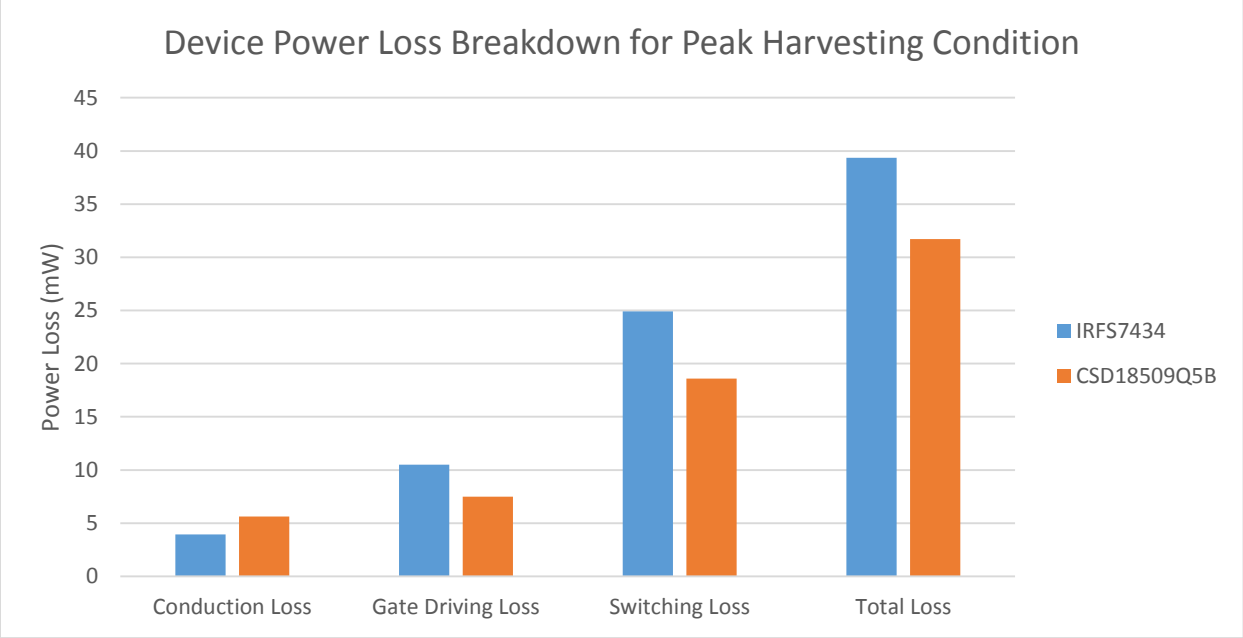

Figure 3.12 Power loss breakdown under peak harvesting condition (V_{in} = 15 V).

3.6 Chapter Summary

This chapter describes the proposed converter design and highlights the steps necessary to prototype with discrete components. The power stage of the converter is designed to minimize conduction losses. The controller is designed to extract maximum power from the harvester through a constant input impedance control mode and protect the battery through an

output regulation mode. LTSpice was used to select certain component values as well as confirm proper operation of the one-cycle control scheme and mode selector.

Chapter 4

Experimental Results

This chapter details the results of experimental testing with the inverting buck-boost prototype with control selection between constant impedance, one-cycle control, and overvoltage shutdown modes. The test results show good prototype performance over a large portion of the input voltage range. The prototype successfully executes all desired functions during appropriate periods of input and output voltage levels.

4.1 Measurement Setup

The first step in testing the prototype was to verify operation of the control network and to tune the circuit to proper operation conditions. Every chip used to implement the control network can be isolated from the board power supply and fed its own power individually. This flexibility in the board design was used to obtain the power consumption of each of the chips at different supply voltage levels in order to obtain the overall power consumption of the control network.

The Printed Circuit Board (PCB) of the proposed buck-boost prototype was designed using Easily Applicable Graphic Layout Editor (EAGLE) Software and was populated with a combination of surface-mount discrete components and through-hole interfacing components. The fully populated prototype is shown in Figure 4.1 with all of the main component functions highlighted.

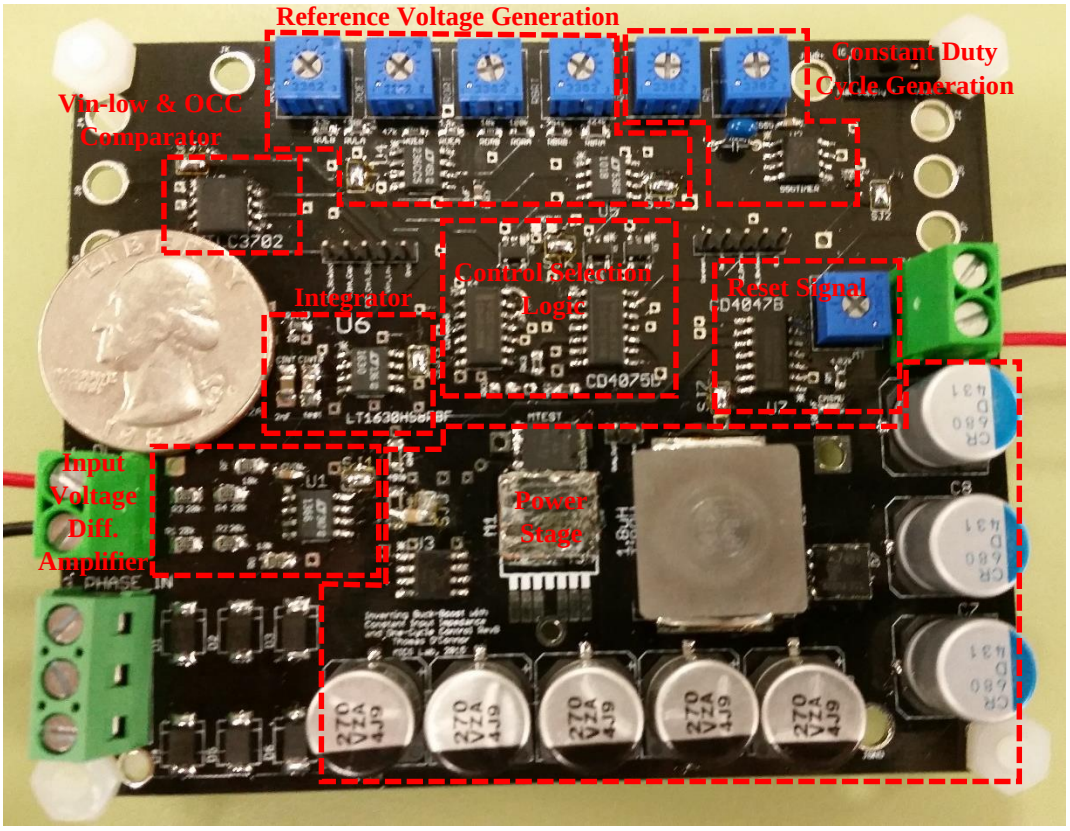

Figure 4.1 Fully populated inverting buck-boost converter prototype with functional blocks highlighted.

In order to test the power consumption of the control network chips, a special board configuration was included in the PCB layout so the power consumption of each individual chip can be monitored. In addition, a SPDT slider switch is used so that the control network can either receive power from the battery at the output or can be wholly powered by a single power supply. Figure 4.2 illustrates both the schematic connections and a section of the board layout which shows the SPDT switch, a solder jumper, and several chip-specific banana jacks. All of the chips can be powered by the same supply if the SPDT is in the appropriate position and all of the solder jumpers are connected. Any IC can be isolated from the power supply by disconnecting the solder jumper and hooking up a separate power supply to the chip-specific banana jack.

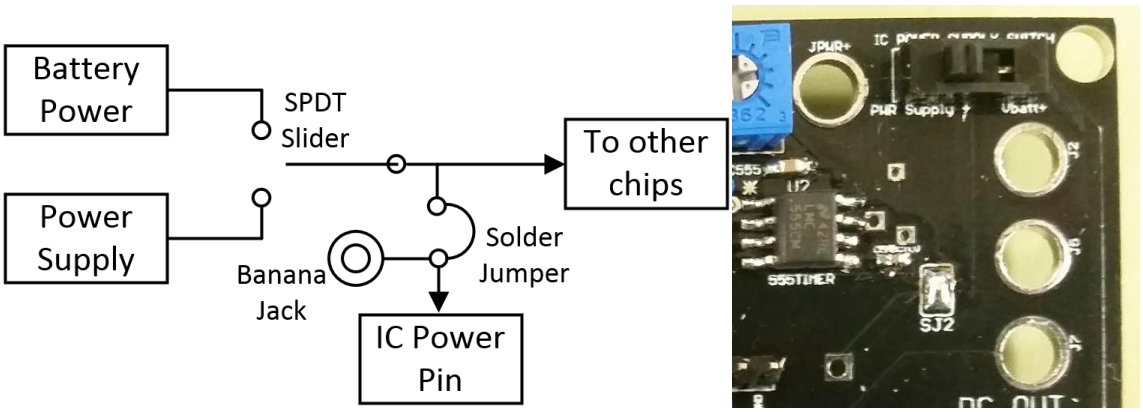

Figure 4.2 Schematic connections (left) and PCB layout (right) for isolating supply power to each of the control network ICs.

After the power consumption of the control network was measured, the performance of the control network was checked for accuracy. The constant duty cycle control was tuned to achieve a constant input impedance of 2 Ω to extract maximum power from the energy harvester. Input voltages were applied to the converter in order to ensure the input impedance produced was equal to 2 Ω. Additional tests were conducted to check the one-cycle control performance. The one-cycle control performance was checked against the ideal calculated duty cycle to assess the accuracy of the duty cycle adjustment in accordance with the input voltage. This test setup was also used to determine accurate transition between the different control modes by varying the input and output voltage levels. Finally, once the power stage was implemented, this test setup was also useful for determining the efficiency and performance of the power stage. Figure 4.3 shows the test setup used to test the performance and power consumption of the control network as well as the efficiency of the power stage.

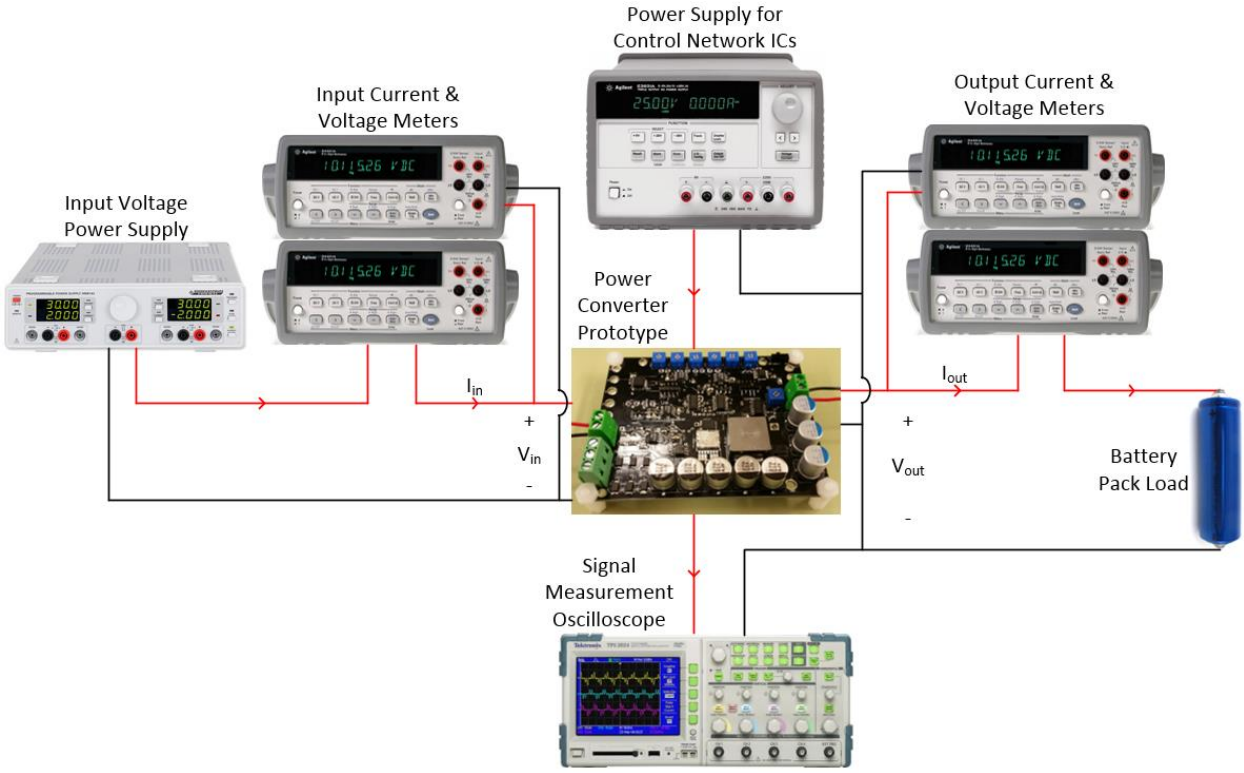

Figure 4.3 Test setup used to measure control network performance, control network power consumption, and power stage efficiency. Figure icons from www.hameg.com, www.agilent.com, and www.tek.com. Used under fair use, 2015.

Finally, once the converter operation had been verified with bench testing, it was necessary to test the entire system: harvester, converter, and battery. Similar to the test process described previously in Section 2.1.1, a hydraulic actuator was used to simulate a controlled displacement of the harvester. The harvester was connected to the 3-phase diode bridge rectifier and a current sense resistor was placed between the rectifier and the harvester to measure input current. Similarly, a current sense resistor was also placed at the output, between the converter and the battery load, to measure output current. Input and output voltage was also measured so that input and output power could be determined under a variety of input voltage levels and while the converter operates in different control modes. Figure 4.4 illustrates the testing protocol used to perform efficiency tests with the harvester, power converter, and battery load.

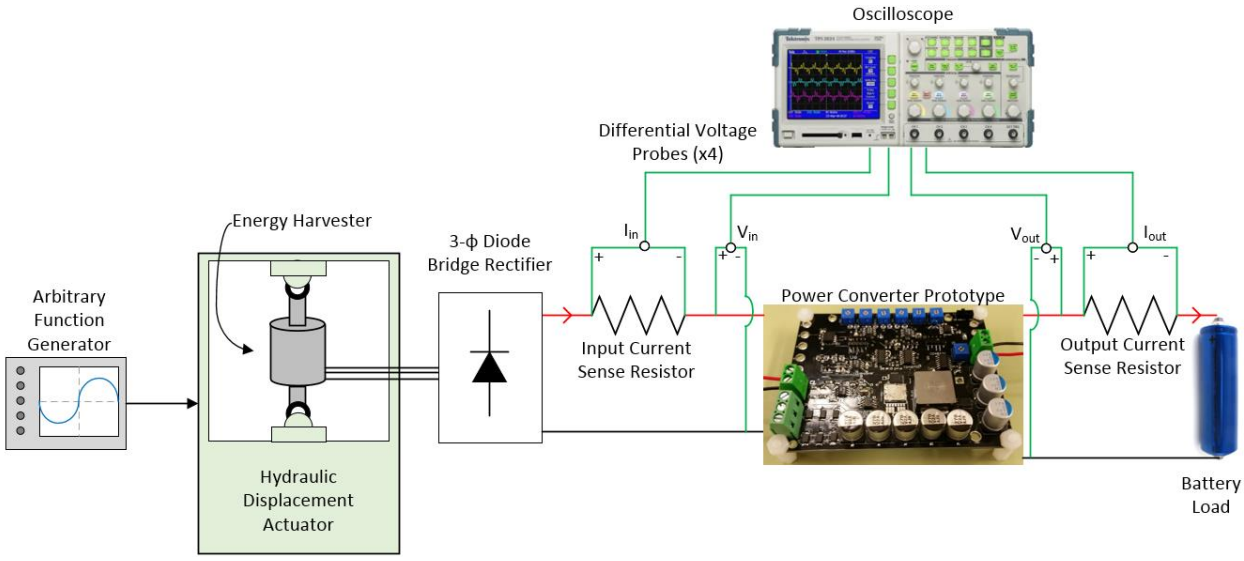

Figure 4.4 Testing diagram for entire system which includes the harvester, converter prototype, and battery load. Figure icon from www.tek.com. Used under fair use, 2015.

4.2 Measurement Results

4.2.1 Control Network Power Consumption

The entire control network was implemented using market-ready discrete components. Each component was chosen based on application-specific criteria. Since the chips will be powered by the battery in the actual application, the supply voltage range was a critical factor in selecting which chips to use. The lowest maximum value of the supply voltage the control chips can handle is 15 V, and the highest minimum value of the supply voltage all the chips can still perform at is 7 V. This voltage supply range was limited by what is currently available on the market and what voltages can be expected from the battery. The battery will only reach down to 7 V if it is very strongly discharged and the converter will shut down once the battery reaches its nominal "full-charge" voltage of 12.8 V.

The discrete components used within the control network consume slightly different amounts of power depending on the level of their supply voltage. Therefore, in order to evaluate the power consumption of each individual component, the chips were all subjected to three different supply voltage levels: 7, 9.5, and 12 V. The results of testing each individual chip in the control network is shown in

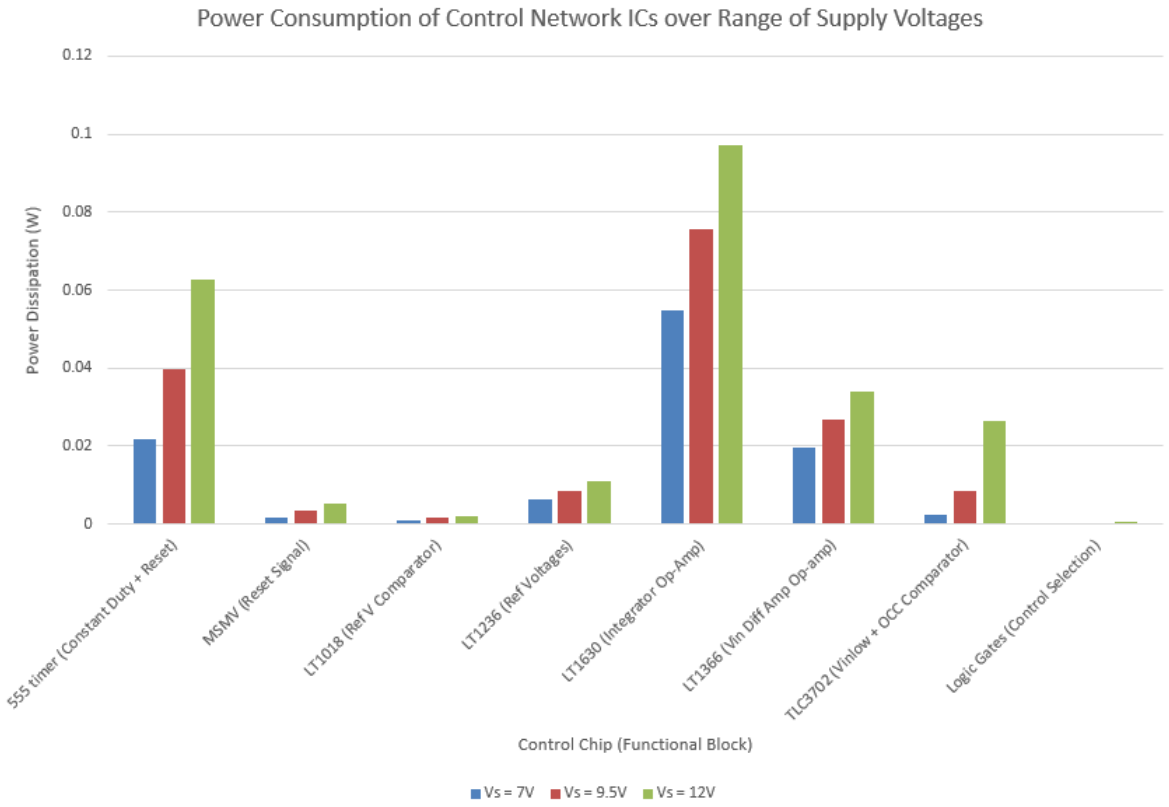

Figure 4.5 Power consumption breakdown of all discrete IC components used in control network.

The most power hungry blocks in the control scheme are also the most essential. The LT1630 op-amp used in the integrator consumes the most power in the control scheme. This is because the bandwidth and slew rate of the LT1630 are both quite high, at 30 MHz and 10 V/µs respectively. This was necessary for proper implementation of the integrator because the op-amp output voltage has to swing very quickly to keep up with the capacitor voltage being discharged over a 1 µs time period. The second most power hungry IC in the control network is the 555 timer. This chip was chosen because it was the simplest way to generate a consistent square wave with 30% duty cycle at 50 kHz which did not depend heavily on the supply voltage. The total power consumption of the control network is 224 mW at a voltage supply level of 12 V. This amount of power consumption is quite low compared to the maximum amount of energy expected to be harvested, and effects the efficiency very little when there is a peak amount of energy to be harvested. The efficiency numbers shown in Section 4.2.3 include the power consumed by the control network with an assumed supply voltage of 12 V.

4.2.2 Control Network Performance

The control network was tested in an incremental testing process before the power stage was added to the prototype. Each functional block within the control network was tested as it was added to ensure functionality of each section. Trim-pots are located on the board to manually adjust reference voltage values, the 555 timer-based constant duty cycle output, and the MSMV reset signal output.

The 555 timer used to set the constant duty cycle and switching frequency was tuned to have a duty cycle of 30% at a frequency of 50 kHz, which translates to an on-time of 6 μs. When this signal is passed to the gate driver, the input impedance to the converter is fixed at 2 Ω. The constant duty cycle signal was also sent to the MSMV to produce the reset signal at 50 kHz. The MSMV was tuned to produce a reset signal with a 5% duty cycle, or 1 μs long, to reset the voltage across the capacitor in the integrator network. The components used in the integrator network were selected to produce duty cycles close to the ideal calculated duty cycle for One-Cycle Control, as discussed in Section 3.4.2. The values within the integrator network were determined primarily by multiple simulation iterations.

Once the functionality of each block in the control network was verified, a power supply was used as the input voltage source, as described in Figure 4.3. A separate power supply was used to provide power to the control network ICs and determine whether the controller was operating in constant input impedance mode or one-cycle control mode. The input voltage power supply was swept over the entire possible input voltage range and the duty cycle was measured with an oscilloscope. Figure 4.6 shows the oscilloscope captures during OCC of the integrator ramp (purple), the duty cycle (green), and the reset signal (gold) for three different input voltage values of 4, 10, and 18 V. Figure 4.7 shows the measured duty cycle as a function of the input voltage compared with the ideal calculated duty cycle for one-cycle control.

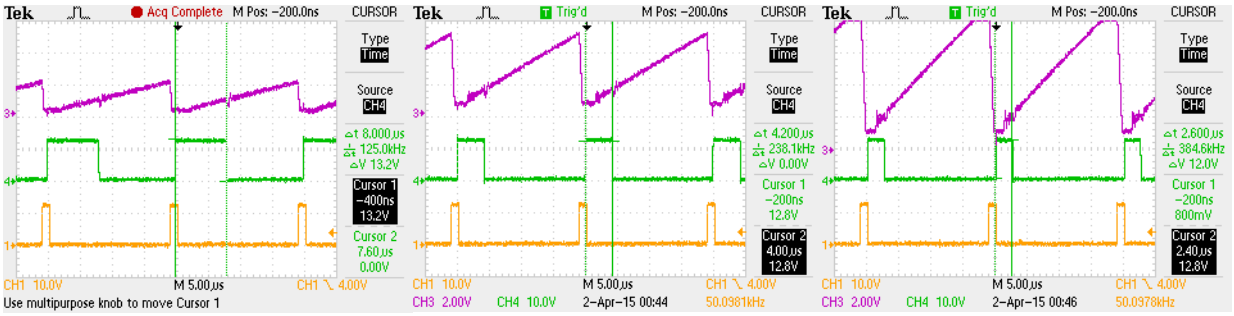

Figure 4.6 Oscilloscope waveforms of the integrator ramp, duty cycle, and reset signals during OCC for input voltages of 4 V (left), 10 V (middle), and 18 V (right).

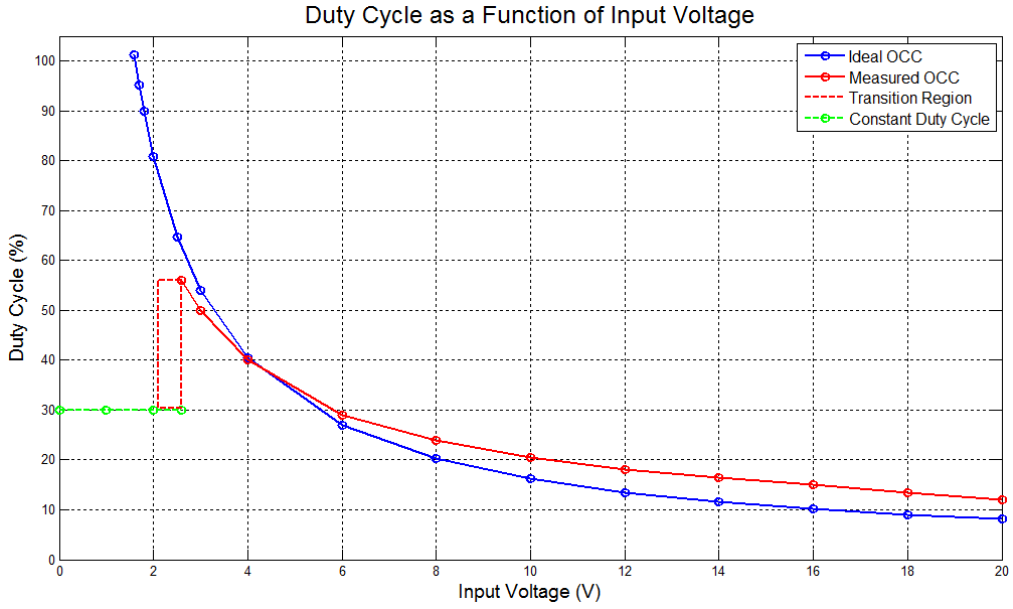

Figure 4.7 Measured duty cycle of converter compared to ideal OCC duty cycle.

Figure 4.7 reveals several important aspects about the proposed control scheme. The first is that one-cycle control does indeed track the input voltage and adjusts the duty cycle on an exponential basis. The component values in the integrator stage can be tuned to adjust the ratio of duty cycle change to input voltage variation. The components used in this prototype yield an OCC duty cycle adjustment that deviates from the ideal calculated duty cycle by no more than 5% of the duty cycle. The transition region occurs when the input voltage being sensed is too low and the $V_{in\text{-}low}$ comparator can be either high or low, depending on the amount of noise present on the sensed input voltage signal. This transition region occurs for an input voltage of 2.1-2.5 V, which represents only 2% of the possible input voltage range. Approaches to alleviate the issue of having a non-clean transition between constant duty cycle control and OCC by adding noise immunity to the $V_{in\text{-}low}$ comparator circuit is addressed in Appendix 1A.

4.2.3 Power Stage Performance

Once the control network performance had been measured and assessed for accuracy, the power stage was installed and tested for overall performance. The range of possible input voltages for bench testing was limited by the current rating of the input voltage power supply, which was limited to 4 A. Since the constant duty cycle mode presents a 2 Ω impedance to the power supply, a maximum of 8 V was able to be measured for the constant duty cycle mode due to the power supply rated current limitation. However, since the duty cycle adjusts during OCC, the input impedance also adjusts, which allows the available power supply to test OCC over the entire input voltage range. Despite the limitation of the power supply, the most important voltage ranges were able to be collected and analyzed. Figure 4.8 shows the measured efficiency for the constant input impedance mode and the OCC mode. Note that the efficiency curves include the power consumption of the control network when a 12 V supply is used (224 mW), as discussed in Section 4.2.1.

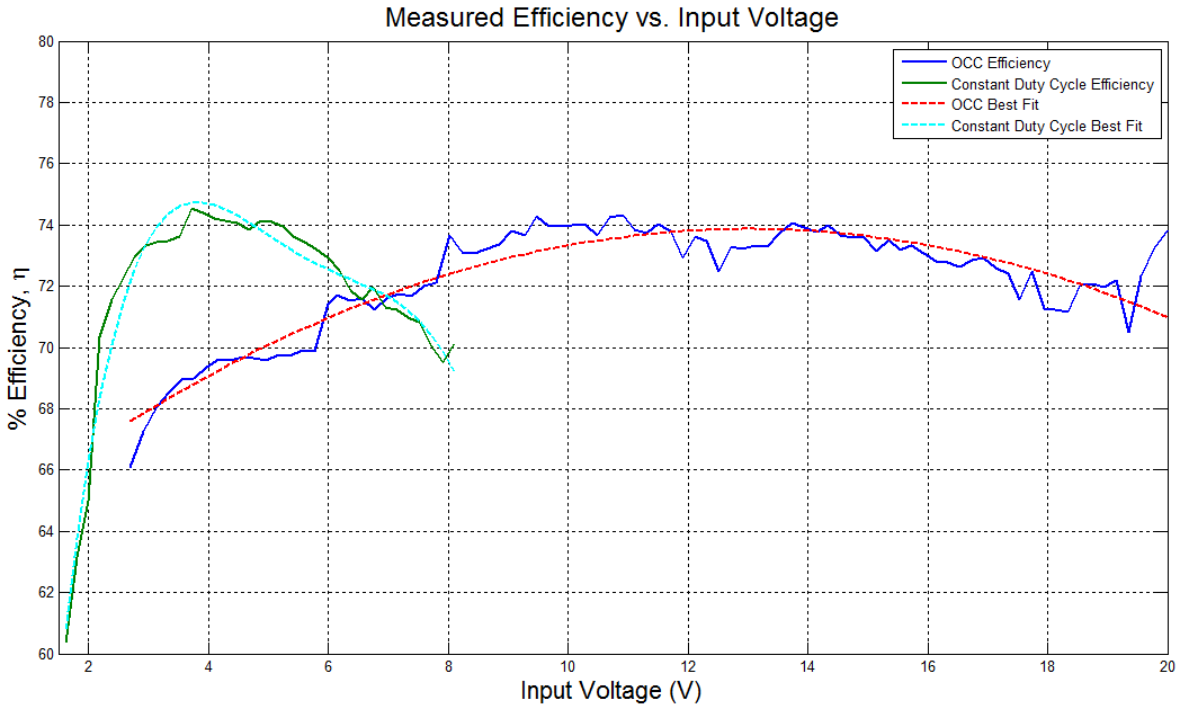

Figure 4.8 Efficiency as a function of input voltage for both control modes.

The plots in Figure 4.8 indicate several important aspects about the power converter. The first, is that the converter reaches a peak efficiency of about 74% for both the constant input impedance mode and the OCC mode. The constant input impedance mode has a much sharper region of peak efficiency, which is to be expected when the duty cycle is not changing. The efficiency for both control modes significantly tapers off at low input voltages because it is not possible to support efficient conversion of such a large step-up in voltage for such a low input voltage and power level. In addition, the power consumption of the control network plays a larger role in affecting the overall efficiency, since the magnitude of power available for conversion decreases with input voltage magnitude but control network power consumption stays relatively constant with respect to the input voltage (control network power is supplied by the battery at the output). This phenomenon results in a positive conversion efficiency for all input voltages at or above 0.9 V with a battery supply voltage of 12 V. The minimum input voltage necessary for positive conversion efficiency would drop to a lower value than 0.9 V if the battery voltage also drops, since the control network consumes less power with lower supply voltage.

The OCC mode is able to extend the higher region of peak conversion efficiency since the duty cycle is allowed to adjust to the optimal value. The transition point at which OCC begins to improve the efficiency is slightly higher than predicted (originally set to ~2 V), but is easily adjusted by changing a reference voltage resistor for determining the $V_{in\text{-}low}$ signal. Moving up the $V_{in\text{-}low}$ transition region shifts the red transition region indicated in Figure 4.7 to about 6 V, allowing for conversion efficiency to be maintained between about 72-74% for a large input voltage range of 3-20 V. Increasing the $V_{in\text{-}low}$ transition region does not damage the battery because the charging current stays below 1 A for input voltages below 6 V during constant input impedance mode.

The goal of the OCC was not only to achieve higher efficiency than the constant input impedance mode, but to also protect the battery by limiting the amount of charging current when the battery is well-charged. When OCC is activated, the amount of current allowed to charge the battery is limited to no more than 1.6 A, which is a suitable maximum for the chosen battery. This maximum charging current occurs at much lower input voltage levels when only the

constant input impedance mode is active. The measured output currents during OCC and constant input impedance mode along with their best fit curves are shown in Figure 4.9.

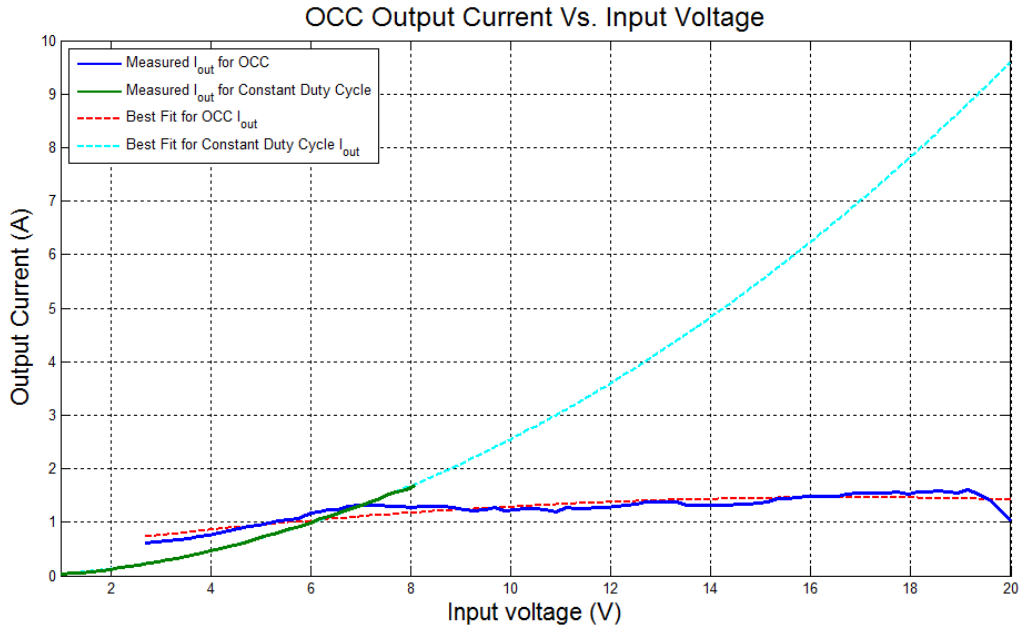

Figure 4.9 Output (battery charging) current for OCC and constant input impedance modes over the range of considered input voltages.

After the converter functionality had been evaluated and ensured, it was important to evaluate what the primary sources of loss are in the converter. A power loss breakdown can be very useful for suggesting the best method of improving the efficiency of the power converter for future studies. Unfortunately, many of the currents flowing through the power stage components cannot be directly measured in this prototype. Thus, the power losses incurred by the resistance in the inductor, diode conduction, and MOSFET conduction and switching losses are generated with simulated results. However, the control network power consumption and gate driver power consumption can be measured, and are included in the power loss breakdown analysis for comparison. Figure 4.10 shows the results of the power loss breakdown analysis.

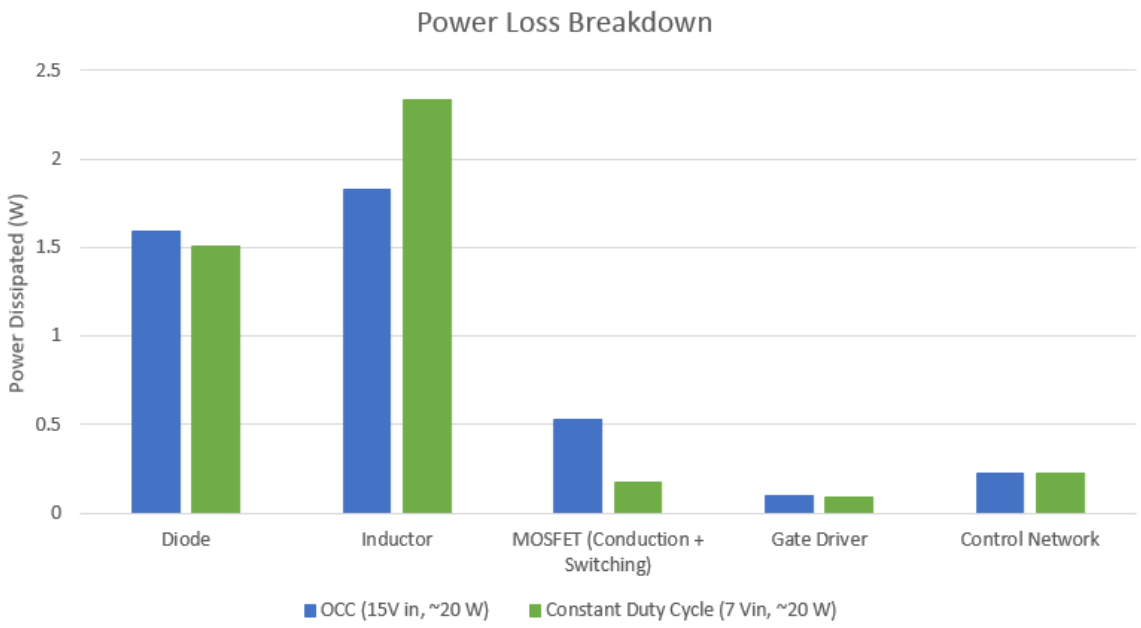

Figure 4.10 Power loss breakdown for converter operating under different control schemes at similar power input levels.

The power loss breakdown yields insight as to where the primary sources of losses occur in the converter. The diode losses make up about 30% of the total loss of the converter under either control scheme, which suggests that a decent improvement in the overall efficiency of the converter could be achieved by replacing the diode with a synchronous p-type MOSFET. The most lossy element, however, is the DC resistance (DCR) of the inductor. Even though the inductor has a low rated DCR resistance of 2.1 mΩ, the high currents associated with the system which flow through the inductor result in a rather large amount of loss. This may be able to be improved by selecting an inductor with a lower DCR resistance; the tradeoff being that the saturation current rating of the inductor will also decrease, which would make the inductor more likely to become saturated, resulting in more loss during peak current spikes. The MOSFET has very low conduction losses due to device selection based primarily on low $R_{ds\text{-}on}$ values. The switching losses make up the bulk of the MOSFET loss, as described previously in 3.5.1, and in congruence with the calculated prediction. Further experiments may be performed to evaluate different MOSFETs and the tradeoff between conduction, gate driving, and switching losses under different energy harvesting levels. The power dissipated by the control network and gate driver can be minimized by combining the discrete components into a single IC control chip, the tradeoff being able to easily adjust the control reference voltages.

4.2.4 Converter Performance with Harvester as Source

Before testing with the harvester began, a comprehensive review of the data taken so far was able to be performed in order to evaluate when maximum power can be extracted from the energy harvester. In order to do this, the input impedance information of the power converter while it is subject to different input voltage levels and operating in OCC mode must be calculated; this is shown in Figure 4.11. As expected, the input resistance of the converter increases as the duty cycle gets smaller due to higher input voltage levels.

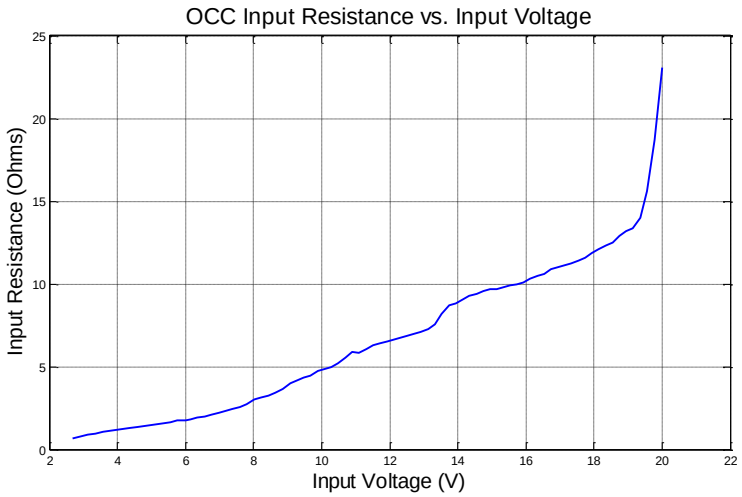

Figure 4.11 Converter input resistance as a result of the duty cycle changing under OCC.

Now that the efficiency and input resistance of both control modes over the entire input voltage range are known, a comprehensive comparison can be made of the total amounts of power able to be harvested and processed by each control system. Using the data of harvester power output vs. load resistance from the 0.5 inch peak-to-peak displacement curve shown in Figure 2.2 and the converter data covered in Figure 4.8 and Figure 4.11, the total amount of power stored in the battery can be evaluated under each of the different control schemes. It is important to note that this is a calculated prediction of when the most energy is harvested for the same amount of displacement subjected upon the harvester and for a relatively constant output voltage which was maintained to obtain the conversion efficiency data. The projected result is shown below in Figure 4.12.

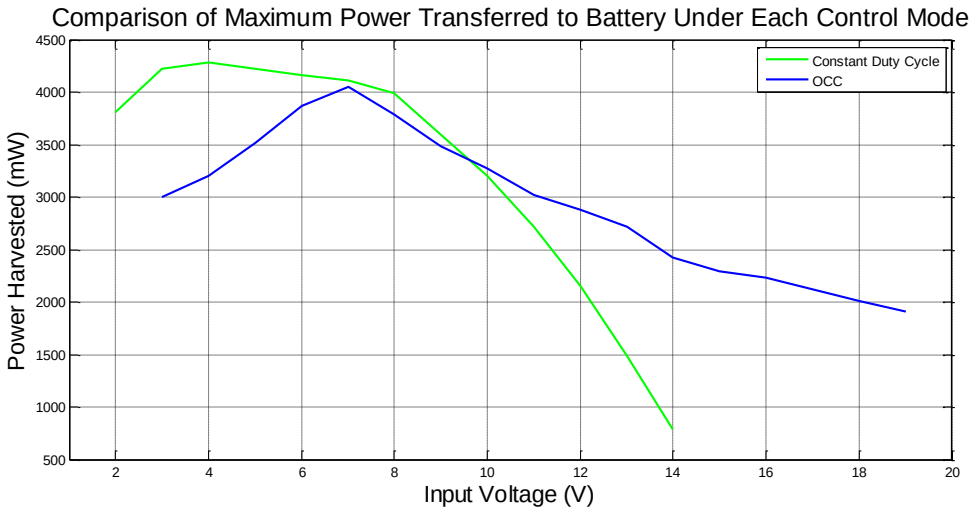

Figure 4.12 Calculated curves used to predict which control scheme transfers the most power to the battery for the same level of harvester displacement.

From Figure 4.12, several conclusions can be drawn. The first is that at a certain point of the input voltage magnitude, the improved conversion efficiency of the OCC mode results in more power being harvested, despite a higher input impedance at the converter causing less power to be extracted from the harvester. The rapid drop off in efficiency at higher input voltage levels causes the constant input impedance mode to harvest less total power, despite extracting the maximum amount from the harvester. Although this prediction may prove slightly unrealistic, since the constant input impedance mode would result in the same input voltage magnitude for a given power level, the result is still pertinent to all possible power levels able to be generated by the harvester. For a fixed power level which would result in an input voltage level of 10 V or more for the constant input impedance mode, more power would be transferred to the battery if the converter operates in the OCC mode. This transition point can move, however, depending on the battery voltage level and power input of the harvester. Since the efficiency of both control modes can be affected by the voltage level of the battery, an advanced control scheme may be able to dynamically determine at which input voltage level the total amount of power harvested can be achieved under each control scheme. This discovery not only suggests a way for improving the control scheme to optimally harvest energy, but also indicates that there is indeed a point where abandoning maximum power transfer in the hopes of achieving higher conversion efficiency results in more total energy being harvested. Implementing such a control scheme, however, would be dependent on thorough testing with the harvester and converter and different displacement and battery voltage levels.

Actual testing with the harvester, converter, and battery load proved much more straightforward and yielded expected results. The testing protocol diagram has been illustrated in Figure 4.4 and a photograph of the test setup is shown below in Figure 4.13.

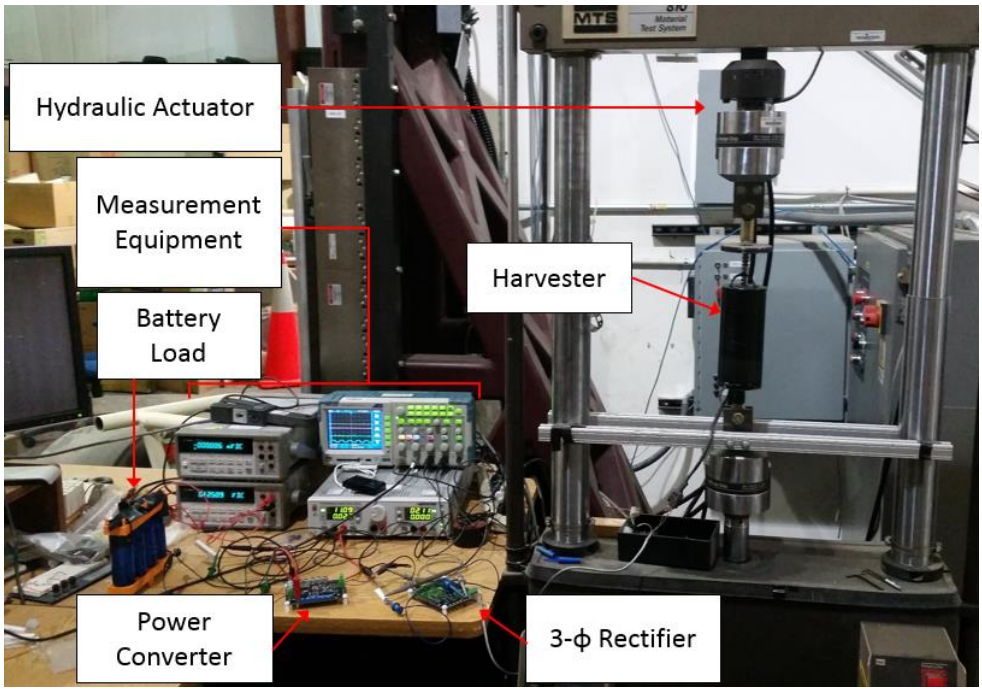

Figure 4.13 Photograph of complete system testing setup.

The harvester, converter, and battery were tested under a variety of different displacement levels so the harvester could send multiple power and voltage levels to the converter. The input current, input voltage, output current, and output voltage information was recorded by the oscilloscope and then post-processed in Matlab to find the input and output power levels of the converter given different harvester-sourced magnitude levels. Figure 4.14 shows the voltage and power at the input and output of the converter operating in constant input impedance mode for a harvester displacement of 0.5 inches peak-to-peak at 2 Hz. Figure 4.15 shows the voltage and power at the input and output of the converter operating under one-cycle control for a harvester displacement of 0.5 inches peak-to-peak at 1 Hz. A number of different harvester displacement magnitudes were used to collect an extensive amount of data and calculate what conversion efficiency the converter is able to achieve under different harvesting conditions.

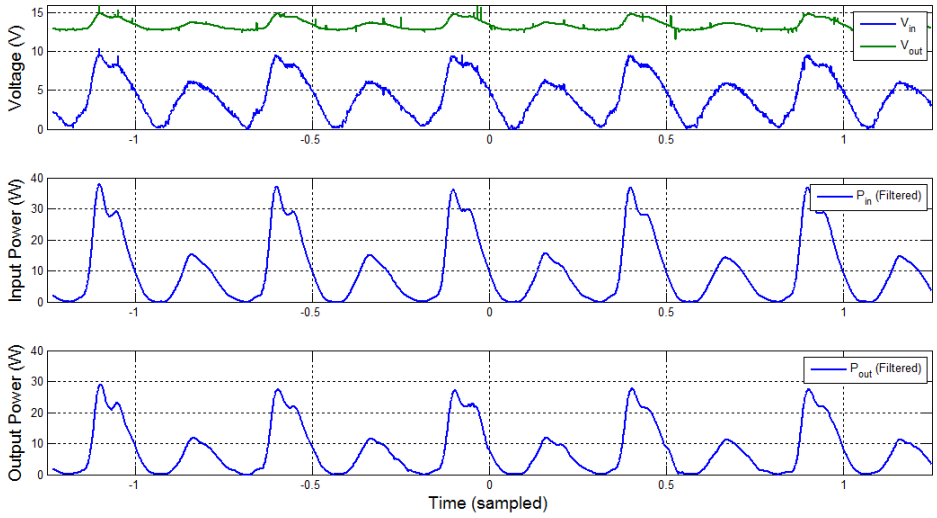

Figure 4.14 Example input/output voltage and power waveforms for the converter operating in constant impedance mode while being sourced by the harvester.

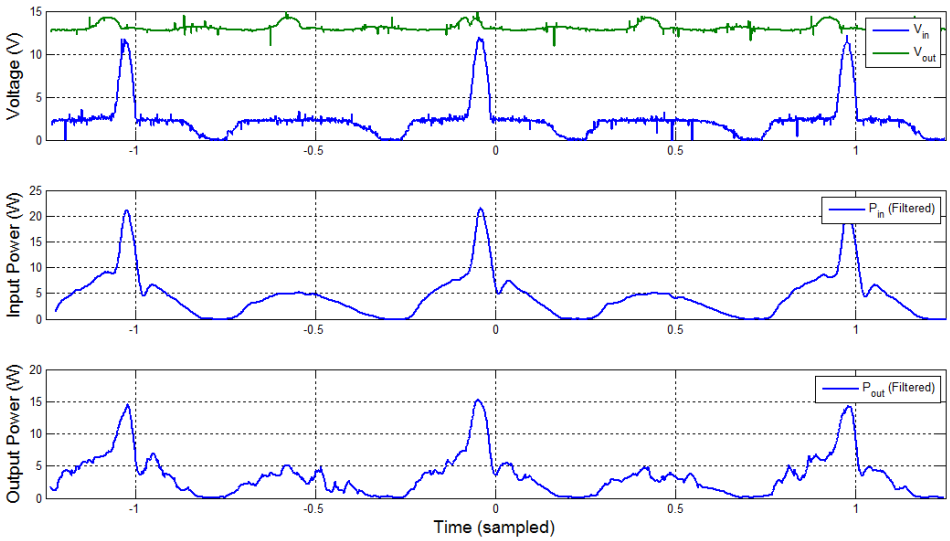

Figure 4.15 Example input/output voltage and power waveforms for the converter operating in OCC mode while being sourced by the harvester.

The waveforms shown in Figure 4.14 and Figure 4.15 reveal a few different discoveries. The first is that the converter is clearly capable of handling the large amount of power the harvester is capable of producing, so the converter is also capable of handling the harvesting peaks seen during real-world track testing. Another discovery is that the waveforms tend to be a bit different, depending on which control mode the converter is operating in. The input voltage magnitude tends to flat-line when the input voltage transitions from being too low (activating a constant duty cycle) to being high enough to activate the OCC mode. This is due to the non-hysteretic $V_{in\text{-}low}$ comparator transition described in 4.2.2, a solution to which is covered in

Appendix 1A. Addressing this comparator transition issue should cause the input/output waveforms to be similar, despite whether the converter is operating in constant input-impedance mode or OCC mode. The rapid increase in input voltage can also be alleviated if the transition between the control modes takes place when their impedances are equal, which occurs when the input voltage is around 6.5 V. Nonetheless, the information from these captured measurements was enough to calculate conversion efficiency as a function of the input voltage sourced by the harvester. The measured converter efficiency when sourced by the harvester is shown in Figure 4.16.

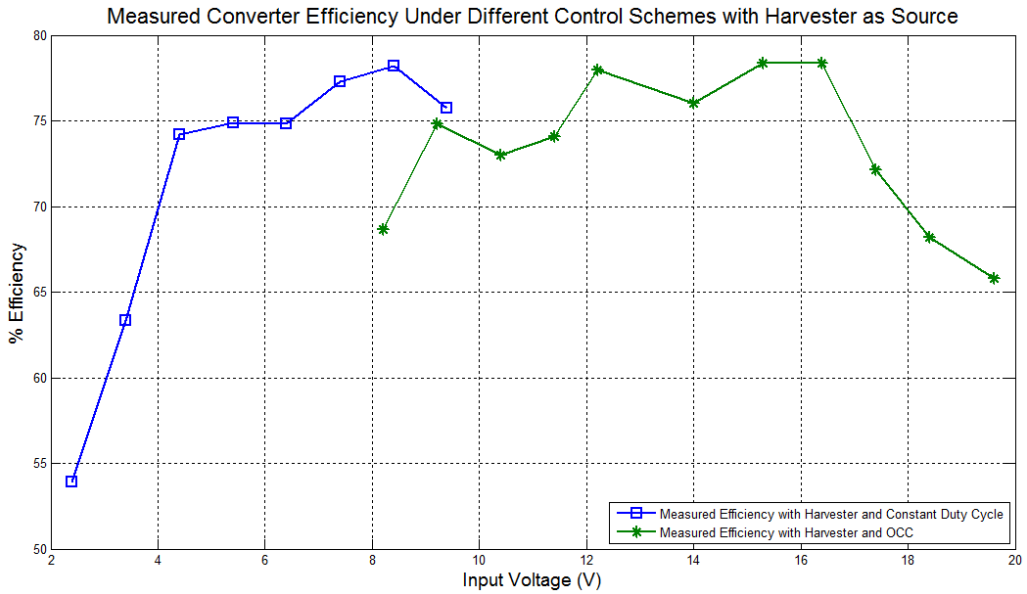

Figure 4.16 Measured converter efficiency as a function of the input voltage sourced by the energy harvester.

The efficiency data recorded in Figure 4.16 yields a similar result to the bench-tested efficiency results. The converter efficiency drops off at low input voltage levels because there is not enough energy being harvested to efficiently push into the battery. In addition, the one-cycle control extends the range of high conversion efficiency to higher input voltage magnitudes. Although the testing equipment did not allow for the harvester to be subjected to larger output voltage levels for the constant input-impedance mode, it can be expected that the efficiency dips down below the OCC efficiency at some point. A final point the harvester-tested data indicates is that the conversion efficiency is slightly higher than the bench-tests and there are a number of different possibilities for this result. First, the current measurements in the harvester-tests are a result of voltage drop over a power resistor; the power resistor heats up during the testing process

which can slightly change the resistance, resulting in a higher resistance than used to calculate the current. Another possible reason is that all factors are being included in the harvester tests, including the effect of the impedance on the power output of the harvester. This can skew the results since the bench-test power supplied was linearly proportional to the input impedance of the converter. Nevertheless, the trend between harvester and bench test data is very similar, indicating proper operation of the entire system.

4.3 Chapter Summary

This chapter presents the fully-operational prototype power converter implemented with off-the-shelf, discrete components. Characteristics of both the control network and power stage implemented on the prototype are discussed in detail. Desired operation of the power converter is tested and verified. Test data is presented which shows the converter efficiency when an ideal source is used as the input and the converter efficiency when the harvester is used as the source input. Possible improvements to the prototype design are suggested throughout the results section.

Chapter 5

Conclusion

A vibration-based energy harvester capable of harvesting energy from a freight railcar's suspension has been developed as a solution to the freight rail industry's desire to electrify their railcars. The desired function of the energy harvester is to charge a battery that can be used to power sensors onboard the railcar. The wide output range and sporadic nature of this energy harvester pose a difficult source for a power converter whose task is to store energy in a battery, but this thesis research investigated a solution. A single-stage power converter is developed which is capable of extracting maximum power from the energy harvester as well as providing battery management features by switching between multiple control schemes. The maximum input voltage to the converter considered is 20 V, and the output voltage range (equal to the battery voltage) is from 7-12.8 V. The predicted real-world harvestable peak power is 72 W, although real-world conditions may provide higher peak power outputs. The converter and harvester were able to be tested together with a maximum of 40 W, but the converter can handle up to 200 W under certain operating conditions.

The proposed inverting buck-boost converter is prototyped using discrete components which can operate off a wide range of single-supply voltages. The control network is designed to operate in a constant input-impedance mode to match the impedance of the energy harvester and extract maximum power when the battery is not well-charged. Once the battery becomes close to fully charged, a battery protection mode is enabled which alters the duty cycle based on the input voltage magnitude in order to regulate the battery charging current. When the battery is fully charged, the converter shuts down to prevent overcharging and prolong the battery life cycle. The efficiency of the converter depends on which control mode it is operating in and what the input voltage and power levels are. Bench-testing has shown peak efficiency to be around 74%, while testing with the harvester has shown peak efficiency of around 78%. The converter can maintain +70% efficiency over input voltage ranges from 2-20 V when operating in the

"nearly-charged battery" region. While the conversion efficiency is not especially high, the control concept has been proven effective in both extracting maximum power and providing battery management in a single-stage converter. This leaves plenty of room to improve the efficiency and further study the optimal transition point between the control schemes.

Future research areas to improve upon for this maximum energy harvesting and battery managing buck-boost converter are listed below.

- Improve conversion efficiency by optimizing components used in the power stage, eliminating the power stage diode by including a synchronous MOSFET, integrating the control network components, and improving board layout to reduce parasitics.
- Investigate different control schemes and evaluate which can most effectively update the duty cycle based on different measured input and output parameters.
- Provide seamless transition between control modes by including hysteresis in control selection signal comparators.
- Compare the effectiveness of an optimized single-stage, multi-control converter to a two-stage converter for energy harvesting and battery management applications.

The above items are left for future research studies on power converter design for vibration-based energy harvesting and battery management.

Appendix

A. Vin-Low Transition Comparator

The transition region between constant duty cycle control and OCC, which occurs when the input voltage is too low to support OCC, is primarily due to the $V_{in\text{-}low}$ comparator being affected by noise from the input voltage differential amplifier. The noisy comparator signal results in an inconsistent duty cycle output during the transitional region between an input voltage range of 2.1 to 2.5 V. A visualization of this problem is shown in Figure A.1, where at the beginning of the transition region, the comparator is mostly low except for when noise causes it to output a high signal level. In the middle of the transition region, the comparator is right in the middle of being high or low, resulting in an output signal that is high much more often. At the end of the transition region, the comparator primarily has a high output, except when noise causes the output to dip low. This issue can be addressed in a number of different ways.

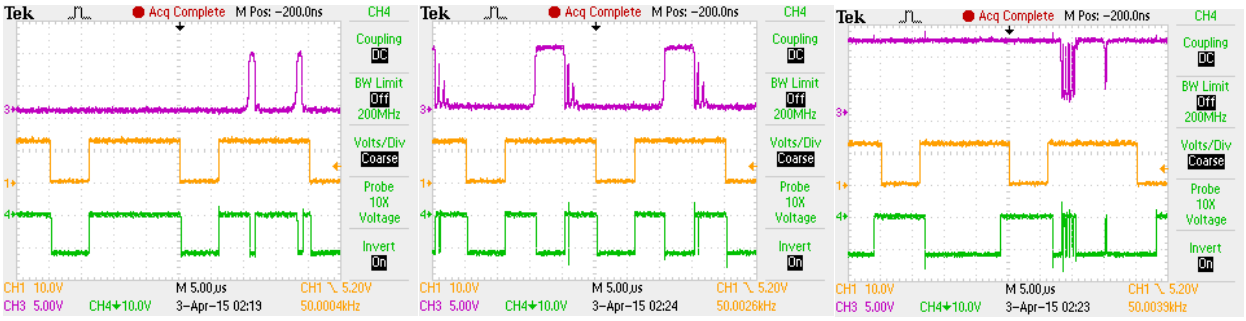

Figure A.1 Noisy comparator signal results in inconsistent duty cycles at the transition period from constant-duty cycle mode to OCC mode for low input voltages. Input voltages equal 2.1 V (left), 2.3 V (middle), and 2.4 V (right).

The first method for addressing this comparator transition issue is to improve the noise level of the sensed input voltage signal. This can be accomplished by optimizing the input voltage differential amplifier or by including larger capacitors for low-pass filtering. While this approach alleviates the issue by lowering the range of voltages which this transition occurs, it does not completely eliminate the issue.

The second method for addressing the comparator transition issue is to include hysteresis on the $V_{in\text{-}low}$ comparator. This would allow for a smoother transition from constant duty cycle mode to OCC mode by having the transition occur at two different voltage levels, depending on if the input voltage was going from high to low or low to high. Discussion on the merits of including hysteresis with comparators to solve instability issues takes place in [31]. The resistive feedback network to achieve non-inverting hysteresis for a single-supply comparator is also described in [31] and is reproduced below in Figure A.2. This type of hysteretic comparator could be used to solve the issue occurring in the $V_{in\text{-}low}$ transition region by setting the hysteretic window to switch to constant duty cycle mode at 2.1 V and to switch to OCC mode at 2.5 V. However, there would likely need to be a voltage buffer at the input to this hysteretic comparator to eliminate feedback from the comparator affecting the sensed input voltage signal.

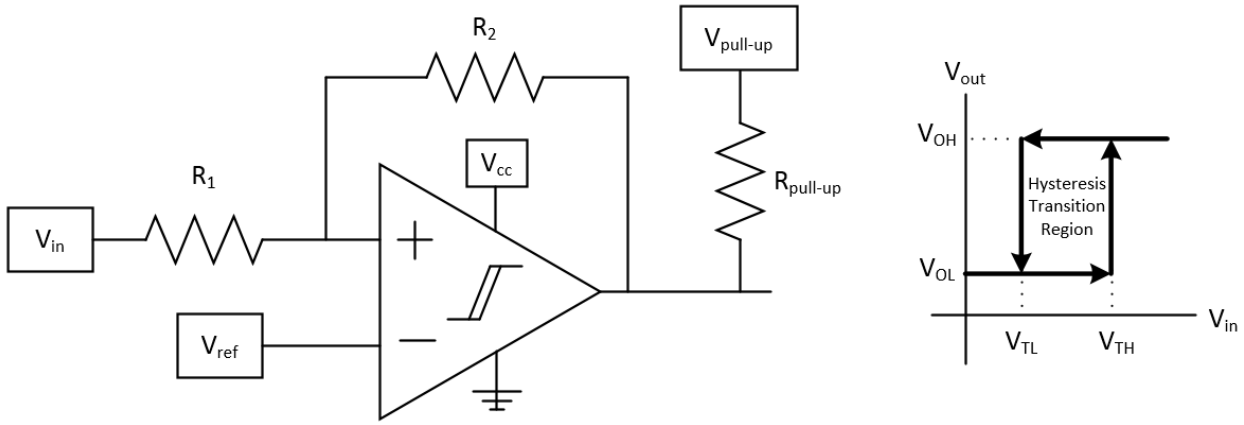

Figure A.2 Non-inverting hysteresis for a single-supply comparator as described in [31].

B. Parts List

Final Parts List for Buck-Boost Prototype				
	Item Description	**Schematic Name**	**Product #**	**Parameter Specifications**
Power Stage	Rectifying Diodes	D1-6	PMEG4050EP	40V, 5A, Vf = 490mV Schottky, SOD128
	Input Capacitor	C1-5	EEH-ZA1V271P	270uF, 35V Os-Con cap
	Output Capacitor	C6-8	PCR1D681MCL1GS	680uF, 20V Os-Con cap
	Top MOSFET	M1	IRFS7434TRL7PP	40V, 240A, 1mOhm Rdson, 315nC Qg
	Alt MOSFET	MTEST	CSD18509Q5B	40V, 100A, 1.3mOhm Rdson, 150nC
	Inductor	L1	IHLP6767GZER1R8M01	1.8uH, 20%, 38A rating, 65A saturation, 2.1mOhm
	Synchronous Diode	D7	STPS30L30DJF	30A, 30V, Vf = 0.3-0.44V
	555 Timer IC	U2	LMC555	1.5-15V supply,
	555 trim pots	RA, RB	3362P-1-103	10k, 0.5W trimpot
	555 timer cap	Ctimer	FK24C0G1H103J	0.01uF, 50V, 5% through-hole cap
	555 filter cap	C555	C0603C104J3RACTU	0.1uF, 25V, 5%, 0603
	Inverting Gate Driver	U3	MIC4429	4.5-18V supply,
Control Selection Circuitry	Triple Input OR Gates	K5	CD4075BM	3ch, 3-input OR Gates, 14-soic
	Quad Input AND Gate	K4	CD4082BM96	3-18V supply, 2 channel, 4-input AND gates
	Inverters (note the inverter for OCC is incorporated in the gate driver)	K1,K2,K3	BU4SU69G2	3-16V supply, single inverter
	Quad Input OR gate	K5	CD4072BM96	3-18V supply, dual quad-input OR gate
	5V Reference IC	U4	LT1236-5	7.2-40V supply, 5V output
	Vbattref Top Resistor	RBRA	ERA-6AEB4643V	464k, 1/8W, 0.1% tol, 0805
	Vbattref Bott Resistor	RBRB	ERJ-3EKF2943V	294k, 1/10W, 1% tol, 0603
	Vref Filter Cap	CREF	LMK107B7105KA-T	1uF Ceramic, 10V, 10%, 0603
	OCCref Top Resistor	RORA	ERJ-3EKF1003V	100k, 1/10W, 1% tol, 0603
	OCCref Bott Resistor	RORB	ERA-3AEB103V	10k, 1/10W, 0.1% tol, 0603
	OCCenable Top Resistor	ROEA	ERA-3AEB332V	3.3k, 1/10W, 0.1% tol, 0603
	OCCenable Bot Resistor	ROEB	ERA-3AEB473V	47k, 1/10W, 0.1% tol, 0603
	Vin_Low Top Resistor	RVLA	ERJ-3EKF1003V	100k, 1/10W, 1% tol, 0603
	Vin_Low Bot Resistor	RVLB	ERA-3AEB332V	3.3k, 1/10W, 0.1% tol, 0603
	Vref 10k trimmers	RBRT,RORT, RVLT,ROET	3362P-1-103	10k, 0.5W trimpot
	OV Shutdown Comparator / OCC Enable Comparator	U5	LT1018	1.1-40V supply, uPwr dual comparator

One Cycle Control Circuitry	Vin Extra Op-Amp Dividers A/B	RHA,RHB	ERA-6AEB4993V	499k, 1/8 W, 0.1% tol, 0805
	Vin voltage follower op-amp	U1	LT1366	1.8-15V supply Rail-Rail In/Out op amp
	Vin Follower Resistor (40k)	R1-R4	ERA-6AEB203V	20k, 1/8W, 0.1% tol, 0805
	Vin Follower Resistor (10k)	RG,RF	ERA-6AEB103V	10k, 1/8W, 0.1% tol, 0805
	Vin Follower Cap (.1uF)	CVIN	C0603C104J3RACTU	0.1uF, 25V, 5%, 0603
	Non-inverting integrator op-amp	U6	LT1630	2.6-36V supply Rail-Rail In/Out op amp
	Integrator resistors	RINTA-D	ERA-3AEB103V	10k, 1/10W, 0.1% tol, 0603
	Integrator capacitor	CINT	12065A472FAT2A	4700pF, 50V, 1% tol, 1206
	Integrator Reset MOSFET	INTFET	2N7002A-7	N MOSFET 60V, .18A, SOT23
	Reset Signal MSMV	U7	CD4047BM96	3-18V Supply, Dual MSMV, 6.8mA out max, 14-SOIC
	Cap for MSMV	CMSMV	C0603C101F5GACTU	100pF, 50V, 1%, 0603 Cap
	Minimum Resistor for MSMV	RM	ERJ-3EKF4021V	4.02k, 1%, 1/10W, 0603
	Trimmer for MSMV	MT	3362P-1-103	10k, 0.5W trimpot
	Integrator and VinLow Comparator		TLC3702CPSR	uPwr Dual Comparator 8SOIC
Miscellaneous	Harvester 3-pin Input Connector		20020316-G031B01LF	3-pin terminal block, 5mm PCB
	2-pin Connector		ED350/2	2-pin terminal block, 5mm PCB
	Standoffs		4816	Hex Standoff, 6-32 Nylon, 1/2" bottom length, 1/4" top thread length
	Slider Switches		SSA12G	20V, 0.4A SPDT Slider Switches
	Test Point Pins		M22-2511005	1 row, 10 pin, 2mm conn header male
	6-32 Nylon Nuts		9606	5/16", 6-32 thread size nylon nuts

References

[1] U.S. Department of Transportation, *Freight Rail Today,* 2012 Federal Railroad Administration.

[2] C. Nagode, M. Ahmadian and S. Taheri, "Vibration-based energy harvesting systems for on-board applications," *Joint Rail Conference,* pp. Pueblo, CO, March 16-18, 2011.

[3] C. Nagode, M. Ahmadian and S. Taheri, "Energy Harvesting Systems to Power Onboard Railroad Equipment," *ASME 2011 Rail Transportation Division Fall Technical Conference,* pp. Minneapolis, MN, September 21-22, 2011.

[4] C. Nagode, *Electromechanical Suspension-based Energy Harvesting Systems for Railroad Applications,* Dept. Mech. Eng., Virginia Tech., Blacksburg, VA, 2013, 2013.

[5] A. Nagorny, *A simple and accurate method for the experiment performance evaluation of high speed sensorless brushless DC motors,* IEMDC '09. IEEE International, vol., no., pp. 916-921, 3-6 May 2009, Electric Machines and Drives Conference, 2009.

[6] Headway Headquarters, "38120S 10Ah LiFePO4 Single Cell Specification Sheet," [Online]. Available: http://www.headway-headquarters.com/38120s-10ah-headway-energy-cell/. [Accessed 2 February 2015].

[7] R.-L. Lin and R.-C. Wang, "Non-inverting Buck-Boost power-factor-correctoin converter with wide input-voltage range applications.," *IECON 2010 - 36th annual conference on IEEE industrial Electronics Society,* vol., no., pp.599,604, 7-10 Nov. 2010.

[8] V. Vorperian, "Simplified analysis of PWM converters using model of PWM switch, Parts I and II".*IEEE Transaction on Aerospace and Electronic Systems, Vol. 26, no.3, pp. 490-496 and pp.497-505, 1990.*

[9] R. W. Erickson and D. Maksimovic, Fundamentals of Power Electronics, 2nd Edition, New York: Kluwer Academic Publishers, 2001.

[10] N. Thao, T. Thang, M. S.M. and J. Park, "Steady-state analysis of the buck converter for renewable energy systems".*Power Electronics and Motion Control Conference (IPEMC), 2012 7th International, vol.3, no., pp.2245,2249, 2-5 June 2012.*

[11] Y. Roshan and M. Moallem, "Maximum power point tracking using boost converter input resistance control by means of Lambert W-Function.".*Power Electronics for Distributed Generation Systems (PEDG), 2012 3rd IEEE International Symposium, vol., no., pp.195,199, 25-28 June 2012.*

[12] R. D'Hulst, P. Mitcheson and J. Driesen, "Cmos buck-boost power processing circuitry for powermems harvesters," *6th International Workshop on Micro & Nanotechnology for Power Generation and Energy Conversion Applications (PowerMEMS)*, Berkeley, USA, Nov. 29th - Dec. 1st, 2006..

[13] X. Cao, W.-J. Chiang, Y.-C. King and Y.-K. Lee, "Electromagnetic Energy Harvesting Circuit with Feedforward and Feedback DC-DC PWM Boost Converter for Vibration Power Generator System," *Power Electronics, IEEE Transactions on, vol.22, no.2, pp.679,685,* March 2007.

[14] S. Dwari, R. Dayal, P. Leila and K. N. Salama, "Efficient Direct AC-to-DC Converters for Vibration-Based Low Voltage Energy Harvesting," *Industrial Electronics, 2008. IECON 2008. 34th Annual conference of IEEE,* vol., no., pp.232-,2325, 10-13 Nov. 2008.

[15] S. Bandyopadhyay and A. Chandrakasan, "Platform Architecture for Solar, Thermal, and Vibration Energy Combining with MPPT and Single Inductor," *Solid-State Circuits, IEEE Journal of ,* vol.47, no.9, pp.2199,2215, Sept. 2012.

[16] X. Qu, H. Han, S.-C. Wong and C. Tse, "Hybrid IPT Topologies with Constant-Current or Constant-Voltage Output for Battery Charging Applications," *Power Electronics, IEEE Transactions on,* vol.PP,no.99,pp.1,2015.

[17] M. Gonzalez, F. Ferrero, J. Anton and M. Perez, "Considerations to improve the practical design of universal and full-effective NiCd/NiMH battery fast-chargers," *Applied Power Electronics Conference and Exposition, 1999. APEC '99, Fourteenth Annual.,* vol.1, no., pp.167,173, 14-18 Mar. 1999.

[18] R. Cope and Y. Podrazhansky, "The Art of Battery Charging," *Battery Conference on Applications and Advances, 1999. The Fourteenth Annual,* vol., no., pp.233,235, 1999.

[19] J. Amanor-Boadu, M. Abouzied, S. Carreon-Bautista, R. Ribeiro, L. Xiaosen and E. Sanchez-Sinencio, "A Switched Mode Li-ion Battery Charger with Multiple Energy Harvesting Systems Simultaneously Used as Input Sources," *Circuits and Systems (MWSCAS), 2014 IEEE 57th International Midwest Symposium,* pp. 330,333, 3-6 Aug 2014.

[20] K. Smedley and S. Cuk, "One-Cycle Control of Switching Converters," *Power Electrnoics Specialists Conference, 1991. PESC '91 Record, 22nd Annual IEEE,* vol. no. pp.888,896, 24-27 Jun 1991.

[21] W. Tang, F. Lee, R. Ridley and I. Cohen, "Charge control: modeling, analysis, and design," *Power Electronics, IEEE Transactions on,,* pp. vol. 8, no. 4, pp 396,403, Oct. 1993.

[22] Texas Instruments, *"LMC555 CMOS Timer",* Feb. 2000 [Revised Jan. 2015].

[23] I. Buchmann, "How to Measure Internal Resistance," Battery University, March 2011. [Online]. Available:

http://batteryuniversity.com/learn/article/how_to_measure_internal_resistance. [Accessed 12 February 2015].

[24] R. C. Jaeger and T. N. Blalock, in *Microelectronic Circuit Design, 4th Edition*, New York, McGraw-Hill, 2010, pp. 565-567.

[25] M. W. Leach, "Ideal Op Amp Circuits," [Online]. Available: http://users.ece.gatech.edu/mleach/ece3050/sp04/OpAmps01.pdf. [Accessed 12 February 2015].

[26] R. Nowakowski and B. King, "Choosing the optimum switching frequency of your DC/DC converter," *EE Times*, 25 October 2006.

[27] D. Jauregui, B. Wang and R. Chen, ""Power Loss Calculation With Common Source Inductance Consideration for Synchronous Buck Converters"," Texas Instruments, 2011.

[28] International Rectifier, "Strong IRFET HEXFET Power MOSFET," IRFS7434-7PPbF datasheet. [Online]. Available: http://www.irf.com/product-info/datasheets/data/irfs7434-7ppbf.pdf. [Accessed 18 February 2015].

[29] Texas Instruments, "N-Channel NexFET Power MOSFETs," CSD18509Q5B datasheet. [Online]. Available: http://www.ti.com/lit/ds/symlink/csd18509q5b.pdf. [Accessed 18 February 2015].

[30] Z. Shen, Y. Xiong, X. Cheng, Y. Fu and P. Kumar, "Power MOSFET Switching Loss Analysis: A New Insight," in *Industry Applications Conference*, Conference Record of the 2006 IEEE, Vol.3, no., pp1438,1442, 2006.

[31] R. Moghimi, "Curing Comparator Instability with Hysteresis.," *Analog Dialogue*, pp. Vol. 34, no. 7, Nov-Dec 2000.